

9/8/80



Lawrence Berkeley Laboratory

UNIVERSITY OF CALIFORNIA

Materials & Molecular Research Division

Submitted to WEAR

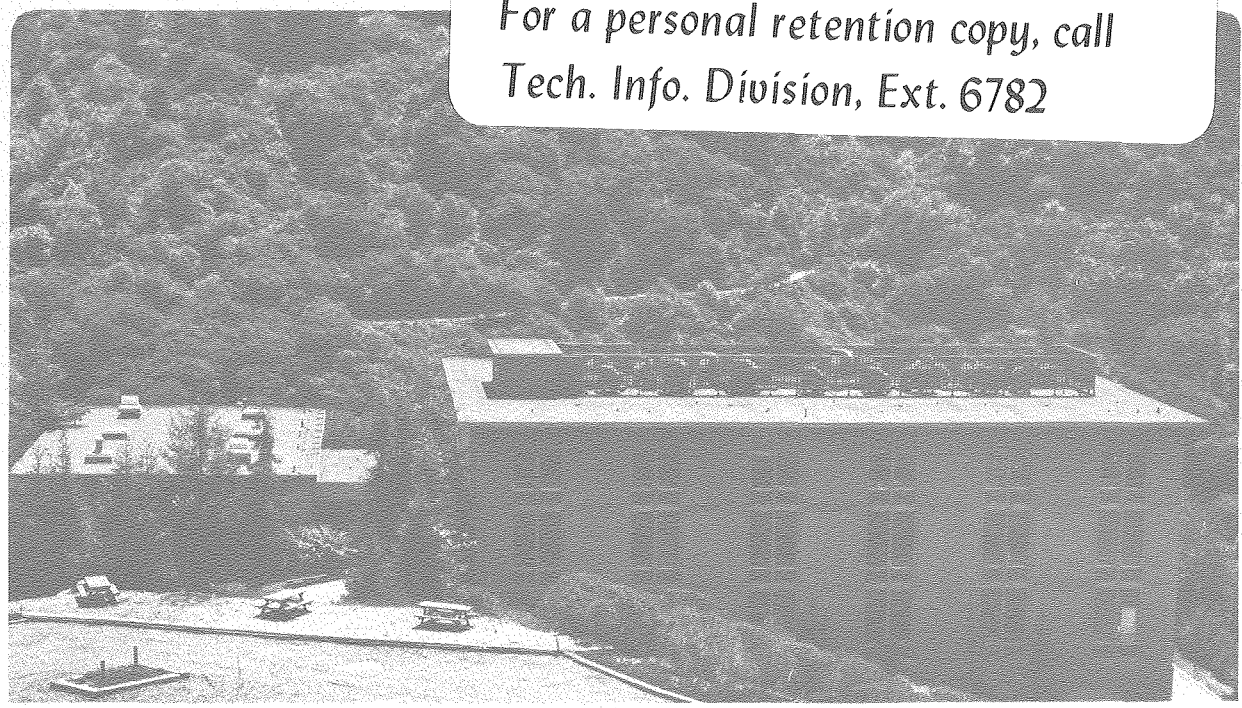
EROSION MECHANISM IN DUCTILE METALS

Robert Bellman, Jr., and Alan Levy

June 1980

RECEIVED
LAWRENCE
BERKELEY LABORATORY
SEP 8 1980
LIBRARY
DOCUMENTS

TWO-WEEK LOAN COPY
*This is a Library Circulating Copy
which may be borrowed for two weeks.
For a personal retention copy, call
Tech. Info. Division, Ext. 6782*



LBL-10289
c.2

DISCLAIMER

This document was prepared as an account of work sponsored by the United States Government. While this document is believed to contain correct information, neither the United States Government nor any agency thereof, nor the Regents of the University of California, nor any of their employees, makes any warranty, express or implied, or assumes any legal responsibility for the accuracy, completeness, or usefulness of any information, apparatus, product, or process disclosed, or represents that its use would not infringe privately owned rights. Reference herein to any specific commercial product, process, or service by its trade name, trademark, manufacturer, or otherwise, does not necessarily constitute or imply its endorsement, recommendation, or favoring by the United States Government or any agency thereof, or the Regents of the University of California. The views and opinions of authors expressed herein do not necessarily state or reflect those of the United States Government or any agency thereof or the Regents of the University of California.

EROSION MECHANISM IN DUCTILE METALS

by

Robert Bellman, Jr., and Alan Levy
Lawrence Berkeley Laboratory
Berkeley, California 94720

This work was supported by the Materials Sciences Division, Office of Basic Energy Sciences, Department of Energy, under Contract W-7405-ENG-48.

ABSTRACT

The removal of material from the surface of a ductile metal by small impacting particles is a design concern to the builders of synthetic fuels plants that utilize pulverized coal to produce gaseous forms of fuel. A series of room temperature experiments was conducted to determine the mechanism of material removal when an erosive particle stream impacts on a ductile metal surface. 1100-O and 7075-T6 aluminum were used for the target and 600 μm SiC particles moving at a velocity of 100 fps in air for the eroding stream. It was determined that a combined forging-extrusion mechanism that produces small, highly distressed platelets of target material that are knocked off the surface by succeeding particle impacts is responsible for erosion at both low and high impingement angles. The large strains that produce the platelets occur in a thin surface region which is heated near or to the annealing temperature of the metal as a result of adiabatic shear deformation. Beneath the soft surface layer is a region that has been cold worked by impact particle induced plastic deformation. This hard, sub-surface layer, once formed, increases the efficiency of platelet formation at the surface and the erosion rate increases to a constant level. This proposed mechanism is a significant departure from the previously believed micro-machining mechanism of erosion of ductile metals.

EROSION MECHANISM IN DUCTILE METALS

by

R. Bellman, Jr., and A. V. Levy
Lawrence Berkeley LaboratoryINTRODUCTION

The erosion behavior of ductile metals is an important design consideration in synthetic fuels process components. The presence of small particles of coal and char in moving gases creates a hostile environment that has been demonstrated to cause unacceptable levels of surface degradation in pilot plant operations. Recent work in studying the erosion behavior of materials¹⁻³ has relied upon older, established mechanisms of behavior that were based on research performed in the 1950's and 1960's in support of oil catalytic cracking and helicopter engine problems. The mechanisms were based on a micro-machining concept where the impacting particle penetrates the target a small amount, translates along the surface removing material ahead of it in a machining mode and finally leaves the surface.⁴ A refined model was developed for this mechanism by Finnie that utilized the equation of motion of the particle tip to define an amount of target material that was removed.⁵ The scanning electron microscope (SEM) with its capability to achieve great depth of field at high magnifications makes it possible to observe what is physically happening on an eroding surface. This critical instrument was not available to Finnie and others at the time of their pioneering work and they had to speculate on what the physical mechanism was.

The micro-machining model has had several problems in predicting the amount of material lost from a surface under a variety of test conditions. Further, it never was able to properly account for erosion at high impingement angles, $> 40^\circ$, or for the start-up period of erosion when particles strike a fresh surface and do not remove material. Researchers through the years have modified the micro-machining mechanism and model, primarily to account for high impingement angle erosion.^{6,7} They have all tended to use the equation of motion of the particle translating along the surface of the specimen as a starting point for developing an analytical model.

Some investigators have attempted to look at the mechanism of erosion from a physical standpoint. To be able to observe what was happening, they used large single particles, millimeters in diameter, and fired them individually at target surfaces^{8,9} or even held the particle fixed and fired the target material at it.¹⁰ In these types of tests, the concentrated kinetic energy from the large mass of the impacting particle was not representative of the much smaller particles (1-250 μm) that occur in real erosion environments. Hence such phenomena as surface melting of the target was observed, an occurrence never seen on actual eroded surfaces.

In work performed at this laboratory^{11,12} several marked discrepancies between the micro-machining mechanism and measured and observed erosion have occurred that became the primary motivation for undertaking the investigation reported herein. The use of the scanning electron microscope (SEM) provided a new dimension to the

insight into what was actually occurring on an eroded surface. This insight was expanded upon and techniques were developed to sequentially observe the erosion process, a particle impact at a time. The erosion regime that was studied involves ductile metals impacted by particles up to 600 μm in size at velocities near 100 fps. In other operating regimes where larger particles and/or higher velocities are used to impact other types of target materials, other mechanisms may occur.

Carefully controlled experiments were conducted where fresh surfaces were eroded on an interrupted basis with SEM observation of the same small surface area between each erosion sequence. This required indexing of the surface so that an area as small as 1000 μm^2 could be precisely relocated after repeated removals and replacements of the specimen on the SEM stage. The result was what is believed to be the first documented history of an eroding ductile metal surface. This painstaking experimental work showed that the basic removal mechanism was not micro-machining but rather a combined forging-extrusion action that produced thin platelets of highly distressed metal that were finally knocked off the surface by succeeding particles.

Seven coordinated experiments were carried out on 1100-0 aluminum, a low strength, single phase, FCC metal and 7075 T6, a high strength, multi-phase FCC aluminum alloy. The 1100-0 aluminum is similar in microstructure and strength at the ambient erosion test temperature to the 300 series stainless steels used in coal gasifier internals at elevated temperatures near 1000°C. The 7075-T6 aluminum alloy at its high room temperature strength can be compared to the low strength 1100-0 aluminum to relate strength and attendant hardness and ductility to the behavior mechanism. The seven experiments were:

- Experiment 1: Sequential erosion of fresh surface of 1100-0 aluminum
- Experiment 2: Impacting particle behavior
- Experiment 3: Sequential erosion of steady state erosion surface of 1100-0 aluminum
- Experiment 4: Sequential erosion of fresh surface of 7075-T6 aluminum alloy
- Experiment 5: Surface behavior of single impact formed craters on a fresh surface of 7075-T6 aluminum alloy
- Experiment 6: Surface behavior of single impact formed craters on a steady state erosion surface of 7075-T6 aluminum alloy
- Experiment 7: Sequential erosion of steady state erosion surface of 7075-T6 aluminum alloy

DEFINITION OF TERMS

Definitions of the terms that are used in this report to describe features of eroded surfaces are presented in this section.

A fresh surface is one that has not yet been eroded. Usually a fresh surface on a test specimen has been polished to a 1 μm finish. An eroded surface is one that has had any amount of particles impact upon it. A steady state surface has been eroded to the condition where the erosion rate has reached a constant value. The erosion rate is defined as the slope of the mass loss vs the amount of eroding particles curve. It has units of g/g or cm^3/g . For ductile metals the erosion rate becomes constant with time after the initial, lower rate incubation period.

The particle stream, consisting of particles entrained in a moving column of gas, is aimed at the specimen surface at a known impact angle which is the least angle between the line of impacting particle and the plane of impact. Particles within the abrasive stream can have a different impact angle with the target surface than that set between the nozzle and the surface. This effective impact angle can be due to aerodynamic effects, particle geometry or rotation of the particle at the time of impact.

When an impacting particle causes a local depression of the surface it creates an impact crater. The entrance side of the impact crater is the side that the tip of the particle first penetrated the target's surface. The exit side is that side from which the damaging particle tip left the surface. Impact craters are always much smaller

than the particles that cause them so only a portion of a particle enters and exits an impact crater. The balance of the particle provides mass for the total kinetic energy of the particle, its driving force. Impact craters on a fresh surface are of three types: indentation, shear and ploughing craters. Indentation craters have some evidence of the initial surface depressed into their walls and have plastically deformed material raised above the initial plane of the surface, called a hump, on the exit side. Smear craters occur when a flat portion of a particle damages the surface over a large area but only to a shallow depth. Usually a ridge of sheared material is pushed to the exit side. The ridge may be strongly or barely attached to the surrounding metal. Ploughing craters occur when a projecting corner or a sharp point on a particle forces its way deeply into the surface and then translates along the surface for a distance. This causes projecting lips to be uplifted along either side of the crater formed. The traverse of the particle also forms a hump on the exit side.

On a steady state surface two different types of impact craters predominate, smear and indentation. The smear craters are larger than those formed during the initial stages of erosion and do not form ridges. Thin platelets of severely deformed metal that extend outward above the adjacent erosion surface occur along the exit and sides of the smear crater. Without bonding to adjacent surfaces, these platelets are barely anchored to a portion of the smear crater and are very vulnerable to being knocked off. Indentation craters on a steady state surface do not form a hump and tend to be somewhat less deep. The edges of the indentation crater have platelet protrusions similar to those seen on a smear crater.

EXPERIMENTAL CONDITIONS

All experiments were conducted with the room temperature erosion tester designed by G. Sheldon (See Fig. 1). With this device, abrasive particles are introduced into a regulated airstream from a vibratory feeding mechanism. Particles were delivered at a rate of 0.1 g/sec. After mixing, the particle stream passes through a 3/16" ID nozzle to impinge on a specimen. The angle of impingement is easily controlled by rotation of the specimen holder. The velocity of the particles can be changed by varying the pressure differential of the carrier gas between the mixing chamber and the tip of the nozzle. Velocity measurements are made using the rotating parallel disk apparatus.¹³

The abrasive used was 600 μm diam. angular silicon carbide. The impingement angle was either 30° or 90°. The velocity was maintained at 100 ft/sec. Erosion usually occurred in short bursts of 0.1 g to 1 g of silicon carbide. The materials eroded were 1100-0 aluminum and 7075-T6 aluminum. Examples of each specimen are shown in Fig. 2 along with an enlargement of the eroded area of the 7075-T6 specimen.

EXPERIMENTAL TECHNIQUES

Real time microscopic observation of the actual erosion process is not possible. What can be done is to make detailed sequential observations of the target surface after short bursts of particles, noting the microstructural changes particles have made by their impact upon the surface of a specimen. If the condition of the surface is known prior to impact, then whatever changes are caused during a subsequent period of erosion will be known and can be recorded.

A technique termed sequential erosion was developed so that the erosion mechanism could be observed. In this method, an uneroded specimen is marked at a control point with several microhardness indentations. This control point serves as a reference for easy relocation of the same zone on the specimen's surface when it is observed in the scanning electron microscope (SEM) after each succeeding burst of particles. The marked specimen is placed in the erosion tester and a small number of particles, typically 0.1 g or 500-1000 particles, impact the surface. The specimen is then removed from the tester and arbitrary areas within the erosion zone are microphotographed in detail. Usually 1 to 5 areas will be chosen. After this, the specimen is returned to the exact position it occupied previously in the erosion tester and it is again impacted with the same number of particles. The previously selected areas are re-examined with the SEM and the damage caused by this second burst of particles is then microphotographed. The cyclic process of erosion - observation is continued until enough data is gathered, usually 3 to 8 cycles.

The above method is equally well applied to an already eroded surface. In this case, the specimen is first impacted with large numbers of particles to bring the specimen into the constant erosion rate regime. After achieving this steady state surface, the specimen is then referenced with the microhardness indentations. After these preparations, the sequential erosion technique proceeds as previously described.

As testing progressed it became desirable to discover why and how a particular shape of crater was formed by an individual particle. Several unique types of craters had been observed and it was thought that each crater could have been caused by a distinct type of particle geometry. The knowledge that a particular particle shape could be responsible for a known type and amount of damage might be utilized to develop a prediction of weight removal based on empirical equations. These equations would relate erosion rate to the number of particles of certain shapes that strike a specimen, knowing their rate and conditions of impact. To this end, methods were developed to thoroughly observe particle geometries before impact, to locate precisely where on a specimen an individual particle had impacted and to retrieve the particle after impact for further observation.

The observation of single particles is accomplished by mounting each particle on a pin head with the aid of a small quantity of carbon paint solution. Several of these pins are then planted in a cork and attached to an SEM specimen holder (See Fig. 3). To avoid electrical charging of the particles, the assembly must be coated with a very thin, conductive, gold layer and each pin must be electrically connected to the specimen holder because the cork acts as an insulator. Particles can be viewed from all angles by manually rotating the pins. Only the end of the particle that is imbedded in the graphite paint is not observable. The smallest particle that can be viewed using this technique is about 400 μm diam.

To retrieve the particles after impact, a special particle catcher was constructed that completely enclosed the specimen holder, except for a portion above the sample which was left open for a clear particle trajectory. The area below the sample was fitted with a 200 mesh screen that permitted free air flow while containing all the particles. This elaborate set up was needed because the high turbulence in the specimen chamber would cause the loss or contamination of minute particles without the special precautions.

The final problem was to locate on a specimen where any particular particle had impacted. On a polished, uneroded specimen, the single pit mark made by the particle was easy to recognize. The problem was to identify the new crater from the literally hundreds of craters formed in the erosion zone on a previously eroded surface. One way would be to photograph the entire erosion zone, impact the single particle, and then rephotograph the whole surface. A careful comparison between before and after pictures would theoretically locate the new crater but it would be extremely time consuming and impractical because of the large erosion zone and great abundance of craters. The erosion zone has an area of roughly 1 cm x 0.5 cm or about 50 million square microns. A typical crater might be only 1000 square microns in area.

Because of the unsuitability of the above method, another very much easier technique was developed that produced unexpected benefits and greatly enhanced the interpretation of crater formation. The method entails sputtering a very thin gold coating onto the surface of

a specimen. The specimen may be either fresh or steady state eroded. The gold coated specimen is then impacted with the single particle. A careful optical examination of the surface using a low power stereo microscope is then made. The impacting particle causes a certain degree of damage to the gold layer as well as to the specimen. By manipulation under a bright light source it is possible to separate the dull silver color of the damaged gold and aluminum from the brilliant gleam of undisturbed gold. This procedure is very exacting but good results were achieved in all instances. The gold coating has an insignificant effect on the erosion process since gold is very soft and malleable. The coating is also very thin, only about 150 Å thick, and a typical crater depth is usually over 20,000 Å.

For actual observation of craters specialized optical and SEM techniques were utilized. With the optical microscope the use of polarized light and color film were useful aids in data interpretation. Polarized light has the property of reflecting at different degrees of polarization depending on the angle of reflection. For example, if a single crater is formed on a flat, fresh surface and the crater is examined optically using special polarizing enhancement lenses, the deformed area about the crater and the hollowed out area of the crater itself appear as a different color than the surrounding specimen surface. In this manner, uplifted material about a crater can be made to stand out more clearly. The degree of plastic deformation in the vicinity of a crater can be better observed and recorded.

The SEM x-ray mapping technique was also used to determine the distribution of gold coating in and around a crater after impact. An

x-ray map is obtained by a detector counter which collects and records the presence of a specific element, in this case gold, using secondarily excited x-rays that have been generated by the primary electron beam of the electron microscope. The relative amount of the element being analyzed is indicated by the density of dots on the screen that indicate a positive count. A high density of dots means a high concentration of the search element. Few or no dots usually mean that only minimal concentrations of the search element are present. However, there can be conditions in the present use when this is not the case. There are some instances when the secondary x-rays are blocked and cannot be collected because an obstruction in the line of sight of the detector absorbs the x-rays, making it impossible for the counter to record them. Accurate x-ray maps cannot be made of the bottoms of deep craters because the crater walls act as an obstruction and block x-rays (See Fig. 4). The effect is minimized if the crater is shallow but there are generally shadows in the direction of the detector.

All of the photographs used in this report are typical of the mechanism occurring on the surface of the aluminum alloys. No other mechanism than that presented was seen. The sequences were selected to clearly show what was occurring. They were randomly selected as any area observed had to be selected prior to the sequence shown. Some sequences selected did not show the mechanism as clearly as others did and they were not used in this paper. However, they all showed the formation of craters and platelets as depicted in the sequence selected for exclusion in the paper.

EXPERIMENTAL OBSERVATIONS

Experiment 1: Sequential erosion of fresh surface of 1100-0 aluminum

Procedure: A small specimen (1" x .75" x .125") of annealed 1100 aluminum was polished to a 1 μm finish to remove surface irregularities and then eroded with 600 μm silicon carbide particles using the fresh surface sequential erosion technique. The impact angle was 90° and the particle velocity was 100 ft/sec. Specific impact craters were selected for observations that were representative of those being formed overall.

Results: In Fig. 5 the value of the sequential observation technique can be seen. Fig. 5a shows the surface in the region of the locating microhardness indentations after 0.1 g of particles (approximately 500 particles) have impacted the surface. This number of particles has caused varying degrees of damage to approximately 50 percent of the target surface. While all particles ostensibly impacted at 90°, there is a considerable variation in the type and degree of damage that was caused. This is due to the geometry variations of the impacting particles and the rotation of the particles.

The larger magnifications in Fig. 5b,c,d, can be used to follow the various types of damage. The bright particle in the lower right center of the photo is a chip of SiC that was broken off of an impacting particle and embedded itself in the surface. Such occurrences happened infrequently. Examples of impact craters,

indentations, humps, ridges and other defined occurrences can be seen in the photos and their sequences of formation followed as the number of impacting particles is increased. The area within the box shown in Fig. 5b is shown at a greater magnification in Fig. 6. It can be used to gain an understanding of the sequence of damage that takes place.

Figure 6a shows a remaining, triangular shaped portion of a raised hump that was formed on the exit side of an impact crater that can be seen immediately to the left of the piece of embedded SiC in Fig. 5. The remaining portions of the hump to either side of the triangular area were depressed into the craters formed on either side of it by other impacting particles. The slip bands observed in the right hand side crater will be discussed later.

Figure 6b shows that a particle impacted the triangular area and smeared a portion of it to the right. No other impacts occurred in the area as all of the other features remain the same. In Fig. 6c, an additional particle or particles impacted the triangular area. It spread the left hand side of the area out over the adjacent crater, caused two ridges to form and flattened the right hand side portion, initiating the formation of a platelet on its surface. An additional 0.1 gm of particles caused the deformation seen in Fig. 6d. The righthand side portion was further flattened and moved over the center portion of the triangular portion, further developing it into a platelet. The small platelet seen on its side in Fig. 6c was probably knocked off but could have been embedded. The thin top of the triangular portion was knocked off. Further platelet formation can be seen in the ridged portion to the left of the triangular area.

This type of sequential forging of material is typical of how particle impacts deform and flatten the surface material, forming thinner and thinner platelets which become more vulnerable to be knocked off by subsequent particle impacts. Additional examples of platelet formation and removal are discussed below.

Figure 7 shows an indentation crater with a series of slip bands occurring along one side. These bands are observed in 5-10 percent of the craters formed. They generally occur along the walls of already formed craters where a fresh crater has been formed immediately adjacent to them. The particle impact forces that cause plastic deformation of the new crater act on the unsupported surface of the already existing crater, resulting in slip band formation. The depth of these bands down the inclined surface of the existing crater is indicative of the depth to which plastic deformation occurs as the result of a particle impact. The slip bands extend to a greater depth along the old crater wall than the depth of the new crater which formed them. This is an important observation that was used in developing the erosion mechanism.

Another type of slip band deformation can be seen on the indentation crater shown in Fig. 8. All of the surface uplift associated with this crater is on the right hand side. This is an indication that most of the impact force was directed towards the right. The impact angle of the particle stream was 90° but, due to particle geometry and rotation, the effective impact angle of the particle was much less. The action of rotation is very significant in

crater formation and one cannot assume an average condition for the impact angle of the particle stream. Very few craters show uniform plastic deformation surrounding them as might be expected with a 90° impact angle. Most have the deformation concentrated around one edge meaning that the major force of impact was angled.

Figure 9 shows a smearing crater that raised a sharp ridge line. Note that some indentation occurred as evidenced by the impressed surface flaws but that the smearing mode is dominant. The trailing side of the ridge shows the beginning of small platelet formation. These platelets are much smaller than those that form after repeated impacts. They are often seen on the sides of exit humps.

Experiment 2: Impacting particle behavior

Procedure: In this experiment individual, $600\ \mu\text{m}$, silicon carbide particles were carefully photographed to obtain a record of their geometry and condition prior to impact.

Documented particles were then individually projected at a fresh 1100-0 aluminum surface at a 30° impact angle and a 100 ft/sec velocity. After impact, each particle was collected in a particle catcher for study and the damage sustained by the specimen surface was located and recorded.

Results: The initial and final appearance of particle "A" is shown in Fig. 10 (the "x" marks a reference spot). The particle was roughly rectangular and measured $1200\ \mu\text{m} \times 400\ \mu\text{m} \times 160\ \mu\text{m}$. It is very angular and shows no evidence of pre-existing cracks. It's

appearance after impact shows that it is still essentially intact; however, a major crack has formed diagonally about halfway through and a thin flake has been chipped off the 1200 μm side of the particle (the outlined area above the "x"). The region at the end of the particle indented the metal surface and its 160 μm dimension roughly corresponds to the long dimension of the crater formed. The chip was broken off due to the high forces in this area. In general, it was observed that an entire particle does not disintegrate on impact but up to 5 percent can be chipped off.

The indentation type crater formed by the particle is shown in Fig. 11. It is triangular and measures about 160 μm x 10 μm x 20 μm . The hump that is expected with indentation craters is hidden in the photo because of microscope orientation. Indentation is evidenced by the surface void marks that have been pushed into the crater exit side wall by the particle. The entrance wall of the crater was probably smeared by the particle.

There is a flattened edge on the crater where the particle exited; a detail of the edge (Fig. 12) shows striation and score marks. Some of the score marks are at angles to others; there is evidence that the particle was rotating while exiting, inferring rotational velocities prior to impact. This crater, which is representative of the type of deformation observed at $\alpha = 30^\circ$, was not formed by the cutting action of a sharp particle; yet conditions were favorable for a "micro-machining" action.

The second particle is shown in Fig. 13. It was roughly triangular in shape, sharp edged, and showed no evidence of fracturing. The crater formed is shown in Fig. 14. This is a ploughing type crater and resulted from the sharp tip of the particle pushing deeply into the aluminum surface. The lips formed on the sides near the exit extend out over the exit hump. This particle's triangular shape with a large projecting tip was responsible for the deep penetration characteristic of ploughing. The dimensions of the tip correspond to the dimensions of the crater.

In both craters there probably was essentially no volume removal of material. Rather, there was extensive redistribution of the surface by plastic deformation.

Experiment 3: Sequential Erosion of Steady State Erosion Surface of 1100-0 Aluminum.

Procedure: The sequential erosion technique was applied to an 1100-0 aluminum specimen that had been brought to the steady state condition by impacting the surface with 500 g of SiC. After this preparation 0.8 g of silicon carbide was used per cycle of subsequent erosion. The impact angle was 30° and the impact velocity was 100 ft/sec. The particles used in one sequence were retained and observed collectively in the SEM. It was not necessary to individually mount every particle. Instead, they all were placed together on a flat 1" diameter disk that served as a specimen holder.

Results: It was expected that the steady state erosion surface would be severely work hardened by the high strains caused by the continuously impacting particles of silicon carbide. The low ductility of the work hardened material would result in brittle fractures of small pieces of the specimen surface and material loss would be by this mechanism.

The series of pictures in Fig. 15 show the expected mechanism not to be the case. No cracks are visible and deformation occurs through a similar smearing and indentation process to that observed on a fresh surface. Craters and smears have platelet-like edges created by impact extrusion that protrude outward over adjacent material and it is the loss of these platelets that appears to be responsible for weight loss. Repeated deformation of craters forming newer craters is common and some platelets are re-extruded several times before they are knocked off. This is evidence of the high ductility of the severely deformed surface.

An explanation for this deformation is the following: As a particle impacts the surface and produces a crater and a platelet, the kinetic energy that it initially possesses is converted into:

1. Deformation strain energy, which plastically deforms the material.
2. Thermal energy which heats the surface during impact by adiabatic shear and, possibly friction between particle and specimen.
3. Particle rotation energy while in contact with the specimen's surface.
4. Elastic rebound energy that is returned to the particle as it leaves the surface.

Enough of the particle's kinetic energy is converted into heating the surface of the specimen that stress relief or even full annealing of the deformed material occurs. The heating of the surface prevents it from work hardening and actually increases its ductility. Therefore, brittle type fractures are not observed. A steady state erosion specimen has three regions of hardness. There is a thin surface layer (5 to 15 μm thick) in which heating is great enough to stress relieve or anneal the surface and keep it soft. Immediately beneath this soft surface is a cooler zone of work hardened material that increases in hardness with distance from the heated surface region to a maximum level and then decreases. Below the work hardened zone is unaffected material.

Once these three zones are fully established steady state erosion occurs. Particles impact the surface and deform it, producing craters, smears and platelets. The particles easily move through the soft ductile top layer but encounter resistance from the stronger work hardened zone. The particles form platelets in the soft surface zone between them and the work hardened zone by an impact extrusion type mechanism, heating the surface in the process. They also plastically deform some material in the work hardened zone, extending it deeper. After several particles impact the immediate area of a platelet it is sufficiently deformed to be knocked off the surface. Figure 16 is a sketch of the proposed regions.

If the effective angle of impact is small, $<40^\circ$, the predominant mechanism is for the particles to slide across the surface, forming smear craters. If the effective angle is $>40^\circ$ then the particles predominantly form indentation craters.

Direct evidence of the existence of elevated temperatures at the eroding surface is seen in Fig. 17 where a typical impacted particle collected after a run is shown. Portions of many of the impacted particles had a mottled, bubbly formation on them that was very strongly attached to the silicon carbide. EDAX analysis of the formations identified them as aluminum. The aluminum was welded to the SiC particle where it was in contact with the target surface.

The surface heating that occurs during erosion does not melt the target because it is a large heat sink with good thermal conductivity. However, the much lower conductivity and heat sink of the SiC particles causes the aluminum welded to them to melt as the result of the heat generated and flow over the particle's surface.

Experiment 4: Sequential erosion of fresh surface of 7075-T6 Aluminum Alloy.

Procedure: The fresh surface sequential impact technique was applied to 7075-T6 Aluminum using 600 μm particles impacting at 90° with an impact velocity of 100 ft/sec. 7075-T6 was selected because its strength and hardness is several times that of 1100-0 aluminum.

Results: The erosion sequence of an area is shown in Fig. 18. The craters are roughly the same size and the general classification of craters is the same as occurred in the 1100-0 low strength aluminum

with one variation. The impact extrusion of platelets occurs more readily on a 7075-T6 fresh surface than on a 1100-0 Al surface. The sequence shows platelets being re-extruded atop previously formed indentations by new craters. Stress relief or annealing must be occurring as the result of temperature generation for so much deformation to take place. The effective impact angles in this sequence were probably close to 90° . An example of an indentation crater with its hump and very fine platelets in an early stage of generation is shown in Fig. 19. Shear deformation is shown in Fig. 20. All impact craters have a much cleaner appearance in the 7075-T6 aluminum.

The fact that the impact craters of 7075-T6 and 1100-0 aluminum under similar erosion conditions are about the same dimensions is significant since 7075-T6 is 6 times as strong as 1100-0 Al, comparing ultimate tensile strength. A probable explanation is that the particle impact forces are so large that the relative differences in strength of the two aluminums are overwhelmed.

Experiment 5: Surface behavior of single impact formed craters on a fresh surface of 7075-T6 aluminum alloy.

Procedure: This experiment was conducted to further define the mechanism of erosion by angular particles. A means of determining what happens to the surface material in direct contact with the impacting particle was developed. It was used to determine whether a micro-machining mechanism occurs that generates new surfaces.

A 7075-T6 aluminum specimen was polished to a 1 μm finish and then sputter coated with a 300 Å gold covering. The specimen was then impacted with 20 single particles of 600 μm SiC at a 30° impact angle and a 100 ft/sec impact velocity. The particles were not photographed beforehand but they were carefully scrutinized under a low magnification stereo microscope and chosen for their regular size angular edges and uncracked appearance. The particles were all roughly the same size as that of particle A" used in Experiment 2. The shallow impact angle and angular shaped particle were chosen to favor a "micro-machining" type of removal mechanism. After the particles had impacted, the surface was examined optically using polarized light and color film so that there was selective enhancement of the plastic deformation. Representative craters were then observed in the SEM and an x-ray map was made to determine the redistribution of gold in and around the crater.

Results: The crater shown in Fig. 21 is a typical indentation crater formed by a single particle impact. The plastically deformed area extends roughly 5 percent to 15 percent of the crater width out from it on the exit side. It is also observed that on the exit side of the crater the gold coating has been peeled away from the surface (See x-ray map, Fig. 21b). There are no scoring or scratch marks on the surface in the peeled area so it is unlikely that the gold was removed by a scraping action of the particle upon exiting. It could

be the result of very rapid elastic deformation and recovery of the aluminum. The gold layer is never actually bonded to the aluminum surface; so it is not possible for it to be stressed simultaneously with the aluminum. The resulting differential movement between the aluminum and the gold causes the gold to peel off. If the peeling of the gold relates to the elastically strained region of the aluminum beneath it, the deformed region is quite large.

Figure 21b shows a gold x-ray map of the crater. A significant amount of gold on the bottom and walls of the crater was detected. The presence of the gold indicates that the generation of new surface in the crater by the removal of a chip of aluminum via a micro-machining mechanism did not occur. Rather, an indentation forging-extrusion mechanism of the type described earlier occurred. The original surface, with its gold coating was pushed down into the specimen by the action of the particle. This crater has some striation marks within it, probably due to some particle translation/rotation while it was in contact with the metal. The pattern of gold in the map does not follow the striation marks.

The crater in Fig. 22 has higher gold concentrations on its walls and bottom and shows the indentation mechanism clearly. The dark particles are aluminide contaminants typical of 7075 alloy.

All other craters had a similar indentation appearance. There was no evidence of micro-machining in this or in any of the previous experiments. The gold coating technique was instrumental in bringing this point out. It would appear that the cutting of a "chip" by sharp

edges of a particle does not occur in small particle erosion where the particle sizes and their kinetic energy force do not generate the type of forces that can generate new metal surface.

Experiment 6: Surface behavior of single impact formed craters on a steady state erosion surface of 7076-T6 aluminum alloy.

Procedure: Having established the mechanism of crater formation on a fresh surface, a similar technique was applied to a steady state surface. A specimen of 7075-T6 aluminum was eroded to a steady state condition with 400 g of silicon carbide. The resulting surface was then coated with a thin layer of gold and subjected to the individual impacts of 600 μm silicon carbide particles. The particles were chosen, as in Experiment 5, for their uniformity and angularity. Particles were impacted at a 30° angle with a velocity of 100 ft/sec. After impact the crater formed was located and observed using the SEM. A gold x-ray map was taken of each crater to determine the gold redistribution. Polarized light techniques could not be applied since the surface presented widely changing topography and there is a limit to the depth of field available in an optical microscope.

Results: A typical indentation crater is shown in Fig. 23 and an example of a smear crater can be seen in Fig. 24. As in 1100-0

aluminum, these are two basic types of steady state impact craters formed in 7075-T6 aluminum. The dimensions of the craters, however, are somewhat smaller. Both craters show the platelet formation about the edges and the smear crater shows a portion of the platelet about to break off. The highly distressed condition of portions of the platelet in Fig. 24 should be noted. It is at this condition that the platelets become most vulnerable for removal by the next particle to impact them.

Experiment 7: Sequential erosion of steady state erosion surface of 7075-T6 aluminum alloy.

Procedure: The platelet formation mechanism was observed, sequentially, in a specific crater area on a steady state eroded surface. The particle size was 600 μm and the impact angle was 30° . The impact velocity was 100 ft/sec for the first test and 200 ft/sec for the second test. The sequences documented in this experiment were representative of what happens over the entire surface rather than being isolated occurrences.

Results: In Fig. 25a can be seen the initial documented state of the selected crater on the steady state surface. It is a typical indentation type crater with well built up platelets in and around it. Figure 25b shows the crater's appearance after the second charge of 1 g of impacting particles. Note that the platelet shown near the top of Fig. 25a has been removed and some new platelets have appeared at the bottom and to the left side of the photo. In Fig. 26a after an

additional 1 g of particles impacts the surface, a new, small impact crater has been formed at the top of the photo with its small platelets and a platelet on the left side of Fig. 26a has been enlarged. Figure 26b shows the final observed conditions after another gram of particles has impacted the surface. Very little of the original crater's surface remains, only a small hole slightly upright of center. Several new craters with new platelets have formed in its place.

The sequence shows that platelet formation and removal is the primary cause for weight loss. It still remains to be determined how many particles, on average, are needed to form a platelet into the distressed condition where it can be removed by the next particle impact. It is apparent that the number of particle impacts in a precise area change randomly from gram to gram of impacting particles. A new method has been developed to control the precise number of particles impacting a very localized area (comparable to that of Fig. 25, 26).

Figure 27 is an additional erosion sequence on steady state eroded 7075-T6 using the new method that shows the formation and removal of a large single platelet. The deformation caused by each succeeding impacting particle (rather than a small but unknown number) can be positively identified. Figure 27a shows the crater as it was first observed. Note that it is a typical indentation type crater with score marks due to particle rotation. In Fig. 27b an additional impacting particle formed a smear crater below the original crater and

pushed a large platelet out and over the initial crater to the left in the photo. The platelet is still strongly attached to the metal surface because the next two particles to impact the area flattened the platelet and slightly shifted its position, as can be seen in Fig. 27c, but did not remove it. The high deformations indicate that not only the platelet but the bonding material holding it to the surface are still quite soft and ductile even after the severe strains that were generated during the platelet's formation. The platelet is knocked off by the next particle impact as seen in Fig. 27d. Major portions of the original indentation crater that was under the platelet in the earlier photos are still intact, indicating that the platelet did not bond to the surface except at its area of initiation.

Through the entire sequence in Fig. 27 the only significant weight loss in the area was that of the single platelet being knocked off the surface. This loss was caused by a known number of particles. One particle formed the platelet, 2 additional particles extended and flattened it and, finally, a single particle was responsible for knocking it off. Four particles caused the formation and removal of a known quantity of material. With further observations of this type, it should be possible to relate the amount of material loss to the number of particles that impact in a small area and then expand the results to cover the entire erosion surface. Using a statistical analysis that accounts for all occurrences, it should be possible to develop a means to empirically relate the weight of eroding particles to the weight of target material removed for the whole surface.

CONCLUSION

Throughout this investigation, the approach was to observe what was physically happening on the surface of an eroding ductile metal at a microscopic level and then to develop the observations into a consistent, logical mechanism of material loss. This mechanism would be based on documented physical occurrences from the first particle impact to the last. A description of this mechanism follows:

Particles initially impact a stress free surface and cause craters to form of three distinct types; indentation, ploughing and shearing. Each type of crater is present regardless of the impingement angle of the abrasive stream. This is because there is a considerable rotational component of all particles and the effective impingement angle can be different from the free stream angle. While all of the types of craters are formed at all impingement angles, their relative amount of occurrence varies with the impingement angle. At shallow angles when the large horizontal component of the velocity overwhelms the particle rotational tendency, smear craters are dominant. As the impingement angle increases, the ploughing type of crater, which is a combination of the smearing and indentation types of craters, increases in its occurrence. At the higher impingement angles, the indentation crater prevails.

As the particles continue to impact there is a general microscopic roughening of the surface because of plastic deformation caused by the large localized stresses in the immediate areas of the particle impacts. In the process of forming craters, platelets of metal that are locally attached to the crater rim are forged-extruded. Some of

the impact kinetic energy is converted into thermal energy which heats the immediate surface area about each crater resulting in warm or even hot working of the surface and the development of a heated surface zone. This enhances the formation of the platelets. At some depth below the surface the metal temperature decreases to the level where the plastic deformation caused by the particle impacts results in a gradual work hardening of the metal.

Eventually the particle impact craters and their attendant platelets completely cover the surface. At this time particles no longer have a fresh surface to impact against and there starts a gradual increase of smear type craters with platelet formation and measureable erosion (actual material loss) now begins.

As the work hardened zone and the soft surface zone further develop, the resistance of the subsurface work hardened zone to penetration by the impacting particles concentrates the plastic deformation in the soft surface layers. This increases extrusion of metal in the softened zone between the particles and the hardened subsurface region which enhances the generation of platelets. As more platelets are available to be knocked off, erosion increases. When the development of the heated surface and cold worked subsurface zones is completed, the incubation period is over and further erosion occurs by the steady state mechanism of indentation, smearing platelet formation and extension, and the removal of platelets though the action of several impacts. This single mechanism can explain erosion behavior observed in many investigation that previously required several mechanisms to describe. Since the mechanism of platelet formation is a straight forward forging-extrusion mechanism it should be conducive to analytical modelling.

REFERENCES

1. Ives, L. K. and Ruff, A. W., "Transmission and Scanning Electron Microscopy Studies of Deformation at Erosion Impact Sites," Wear 46 (1978), pp. 149-162.
2. Gane, N. and Murray, M. J., "The Transition from Ploughing to Cutting in Erosive Wear," Proc. 5th Inter. Conf. on Erosion by Solid and Liquid Impact, 3-6 Sept. 1979, Cambridge, England.
3. Sargent, G. A., Keshavan, M. K., and Conrad, H., "The Effect of Microstructure on the Erosion by Solid Particles," Metallurgical Engineering and Materials Science Dept., University of Kentucky, Lexington, Kentucky 40506 (1979).
4. Finnie, I., "Erosion of Surfaces by Solid Particles," Wear 3 (1960), 87-103.
5. Finnie, I and McFadden, D. H., "On the Velocity Dependence of the Erosion of Ductile Metals by Solid Particles at Low Angles of Incidence," Wear 48-1, May 1978, pp. 181-190.
6. Bitter, J.G.A., "A Study of Erosion Phenomena," Parts 1 and 2, Wear 5 (1963).
7. Neilson, J. H. and Gilchrist, A., "Erosion by a Stream of Solid Particles," Wear 11 (1968), p. 11.
8. Sheldon, G. L. and Kanfere, A., "An Investigation of Impingement Erosion Using Single Particles," Wear 21 (1972), pp. 195-209.
9. Christman, T. and Shewmon, P. G., "Erosion of a Strong Aluminum Alloy," Wear 52 (1979), pp. 57-70.

10. Winter, R. E. and Hutchings, I. M., "Solid Particle Erosion Studies Using Single Angular Particles," *Wear* 29 (1974), pp. 181-194.
11. Levy, A. V., "The Role of Plasticity in Erosion," Proc. 5th Inter. Conf. on Erosion by Solids and Liquid Impact, 3-6 Sept. 1979, Cambridge, England.
12. Mayville, R. A., "Mechanism of Material Removal in the Solid Particle Erosion of Ductile Metals," M. S. Thesis Lawrence Berkeley Laboratory report LBL-7333, Berkeley, California (1978).
13. Ruff, A. W. and Ives, L. K., "Measurement of Solid Particle Velocity in Erosive Wear," *Wear* 35 (1977), 195.

FIGURE CAPTIONS

- Figure 1. Room temperature erosion tester.
- Figure 2. Test specimens of 1100-0 and 7075-T6 aluminum.
- Figure 3. SEM setup for individual particle examination.
- Figure 4. Sketch showing how surface topography obstructs SEM x-ray detector.
- Figure 5. Sequentially eroded surface of fresh 1100-0 aluminum.
- Figure 6. Initiation of platelet formation in 1100-0 aluminum.
- Figure 7. Presence of slip deformation bands in crater walls of previously formed craters.
- Figure 8. Presence of slip deformation bands in as-formed crater wall.
- Figure 9. Indentation crater showing original surface flaws impressed in crater bottom.
- Figure 10. Initial and final appearance of SiC particle "A".
- Figure 11. Indentation type crater formed by particle "A".
- Figure 12. Detail of edge of crater showing multi-directional score marks.
- Figure 13. Initial appearance of SiC particle "B".
- Figure 14. Ploughing type crater formed by particle "B".
- Figure 15. Sequentially eroded surface of steady state erosion 1100-0 aluminum.
- Figure 16. Sketch of soft surface and work hardened layers with platelet formation and loss.
- Figure 17. Surface of used SiC particle showing evidence of melted aluminum on its impacting surface.

- Figure 18. Sequentially eroded surface of fresh 7075-T6 aluminum.
- Figure 19. Fine platelets of 7075-T6 aluminum in early stage of generation.
- Figure 20. Smear type crater in 7075-T6 aluminum.
- Figure 21. SEM image and gold x-ray map of indentation crater in fresh surface.
- Figure 22. SEM image and gold x-ray map of indentation crater in fresh surface.
- Figure 23. SEM image and gold x-ray map of indentation crater in steady state erosion surface.
- Figure 24. Smear crater with platelets in steady state erosion surface of 7075-T6 aluminum.
- Figure 25. Sequential platelet removal from a smear crater - early stage.
- Figure 26. Sequential platelet removal from a smear crater - later stage.
- Figure 27. Sequential platelet formation and removal by subsequent individual particle impacts.

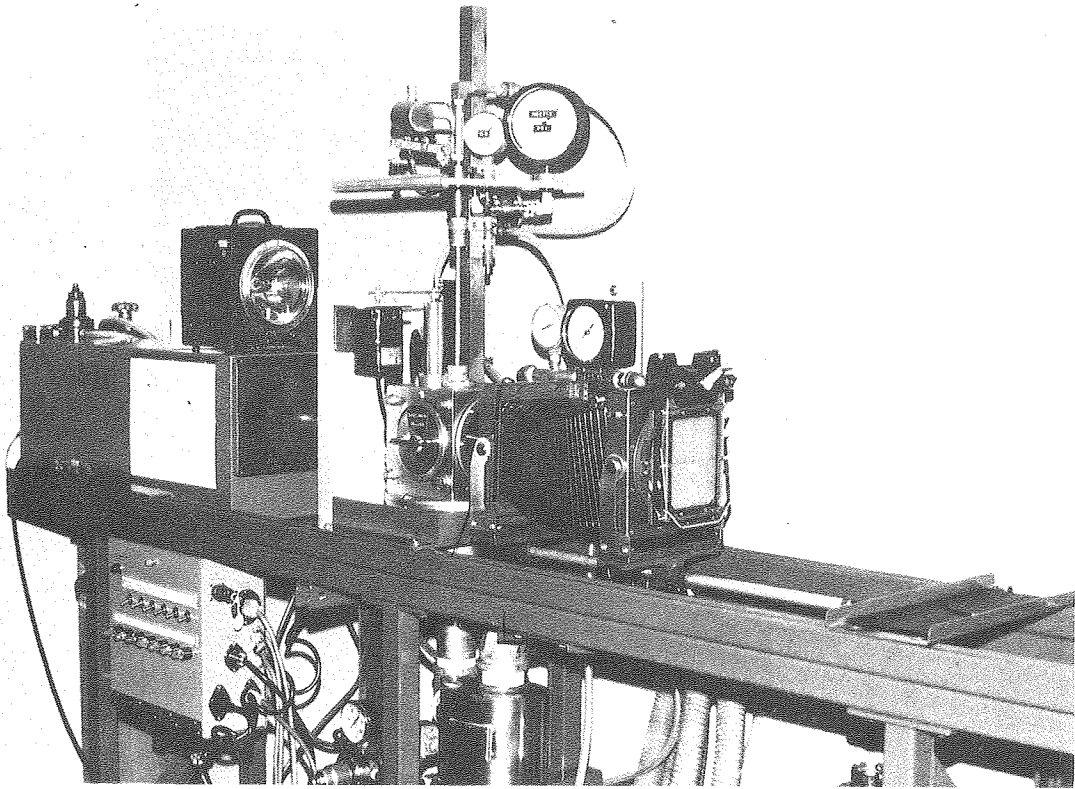
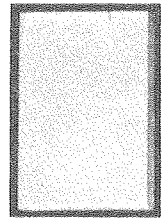


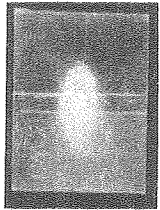
Fig. 1

CBB 763-2073



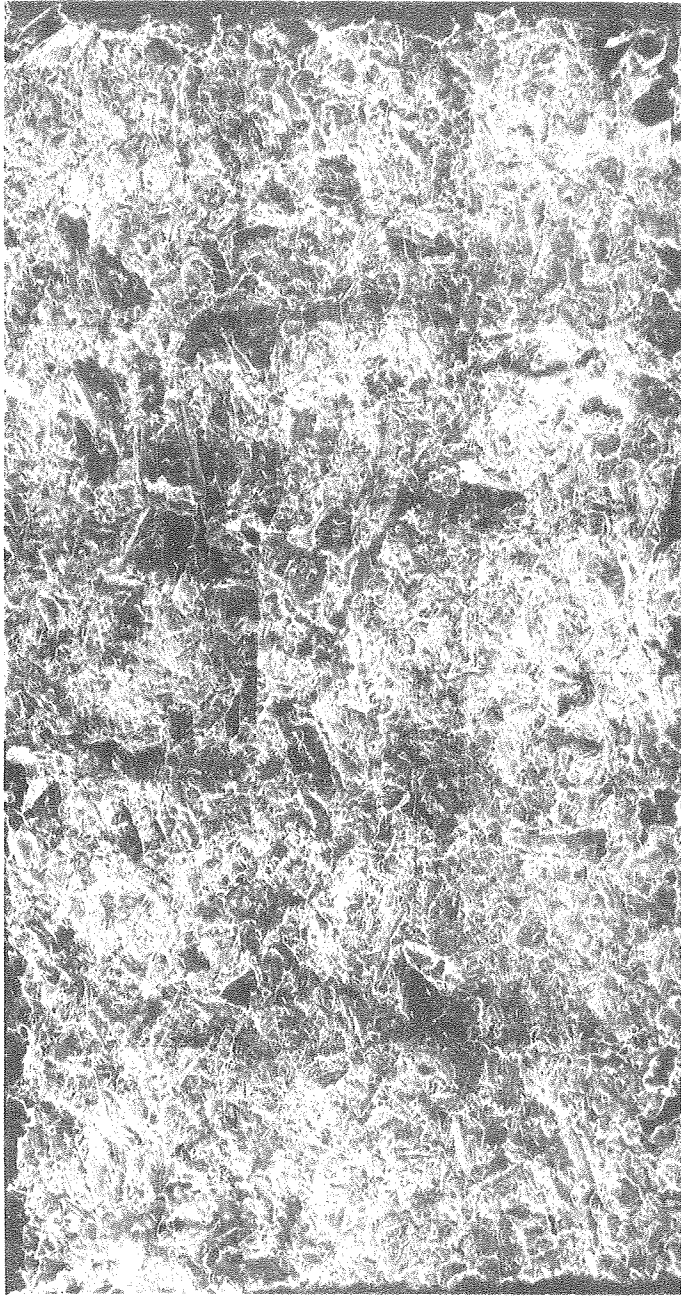
1 cm

1100 Al



1 cm

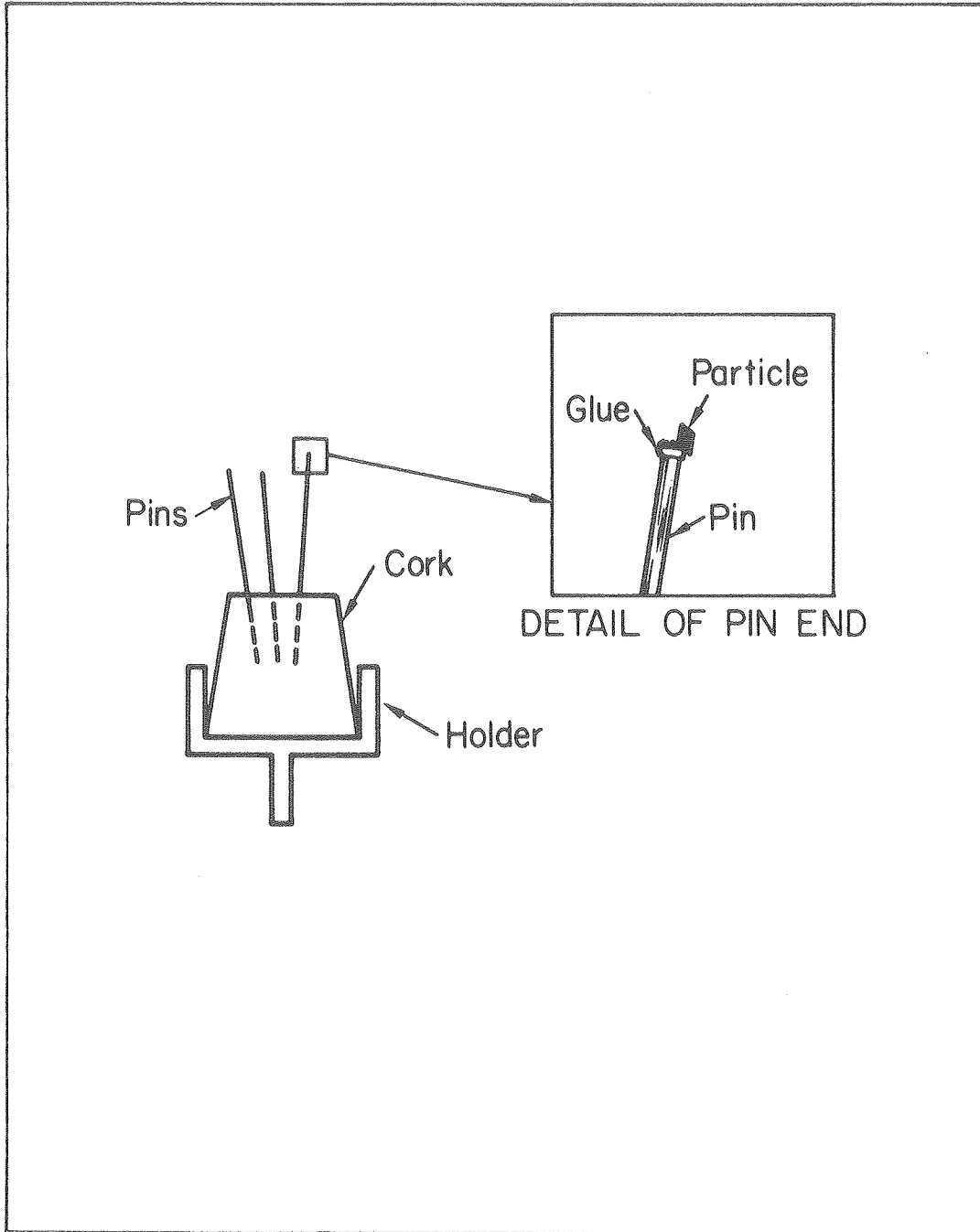
7075 Al



100 μ m

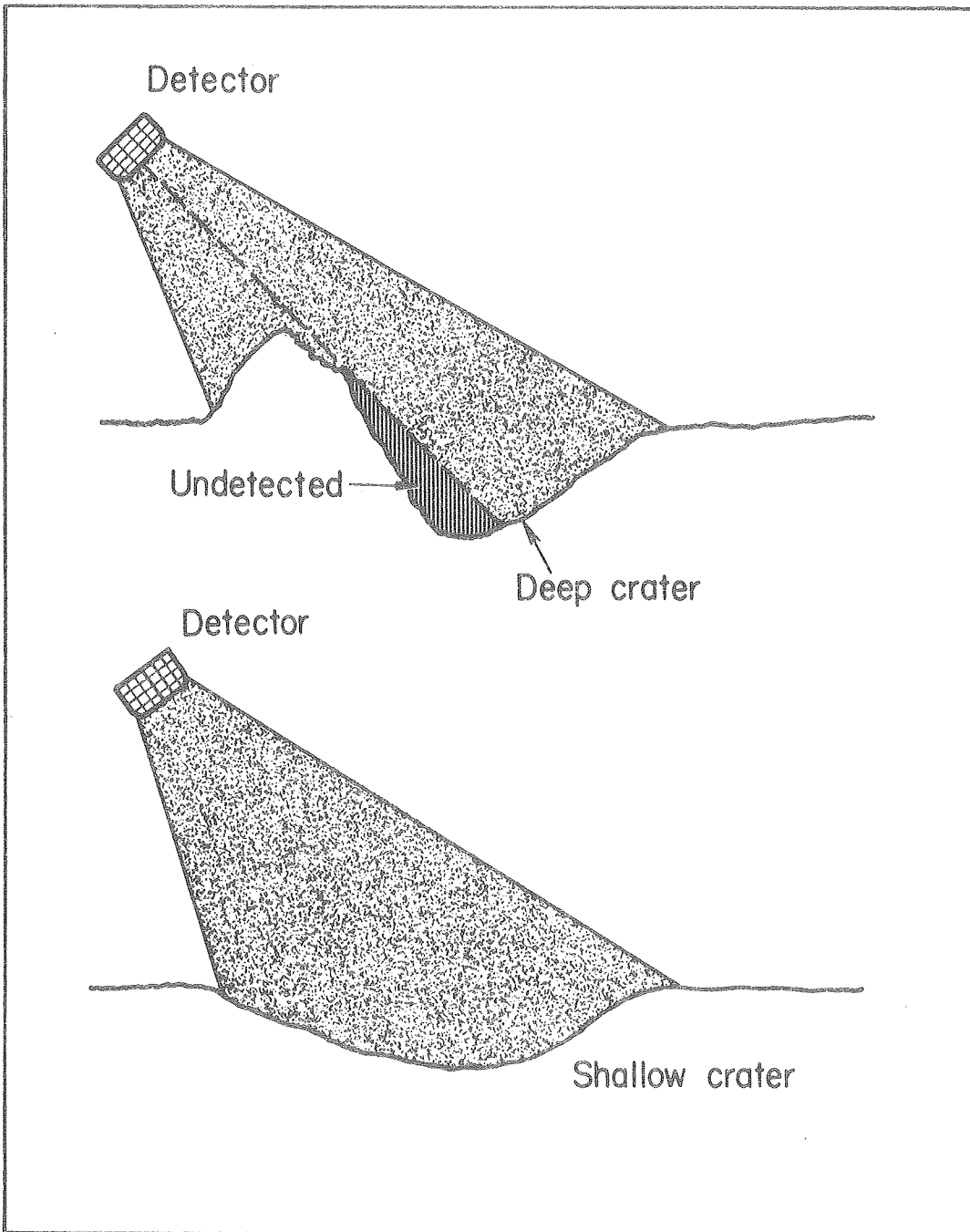
Fig. 2

XBB 806-7868



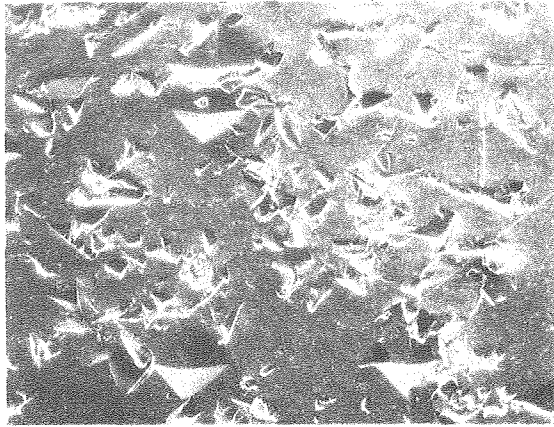
SEM SET-UP FOR PARTICLE EXAMINATION

XBL 807-10670

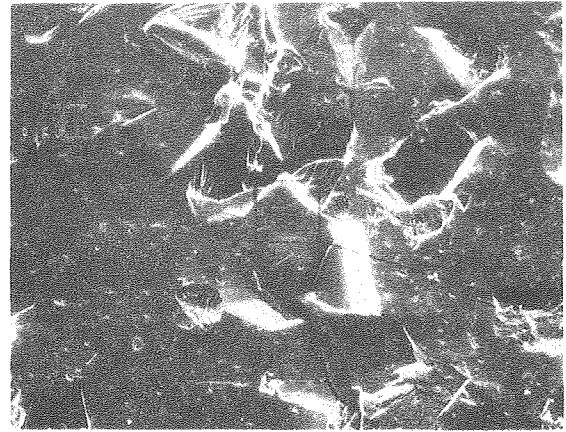


XBL 807-10671

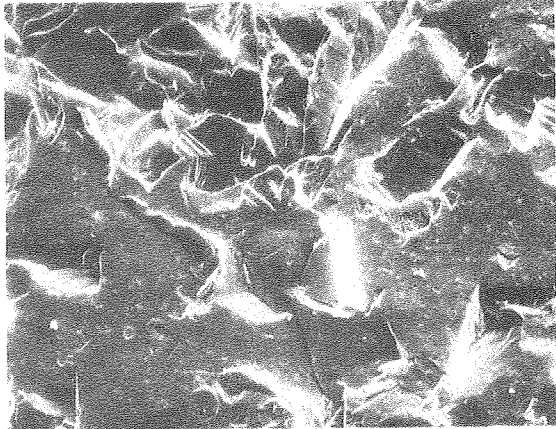
Fig. 4



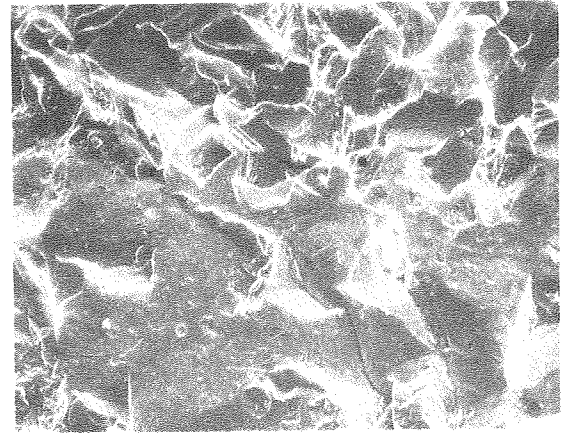
A 0.1 g 200 μm



B 0.1 g 50 μm



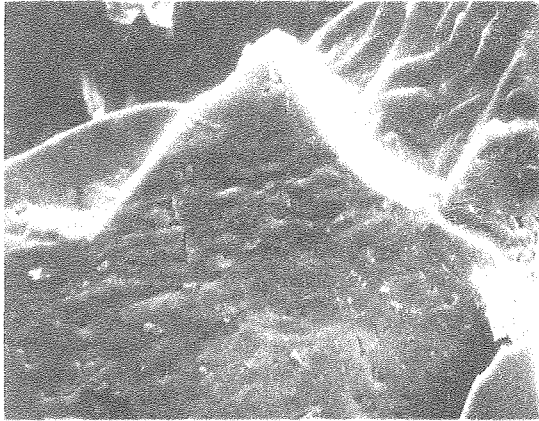
C 0.3 g 50 μm



D 0.4 g 50 μm

Fig. 5

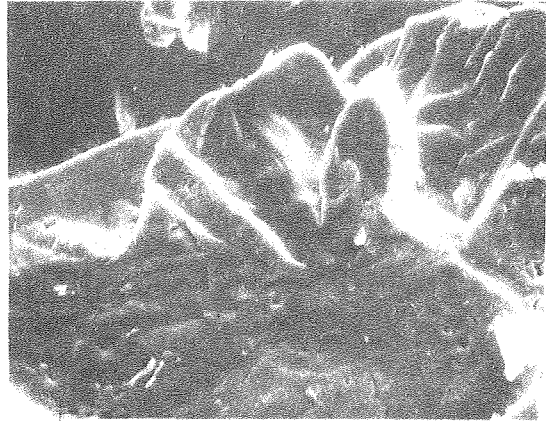
XBB 790-13298A



A

10 μ m

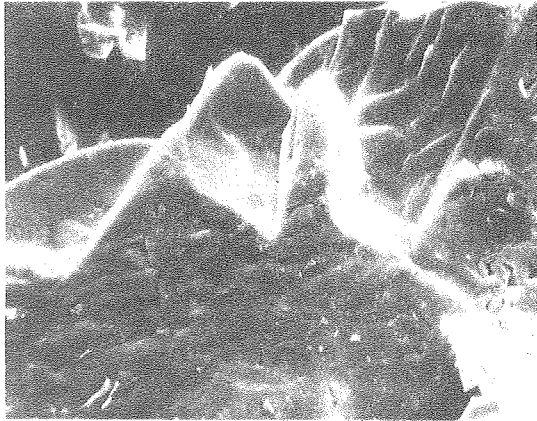
0.1 g



C

10 μ m

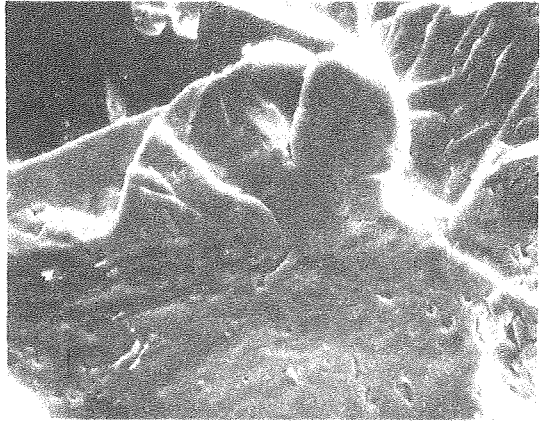
0.3 g



B

10 μ m

0.2 g



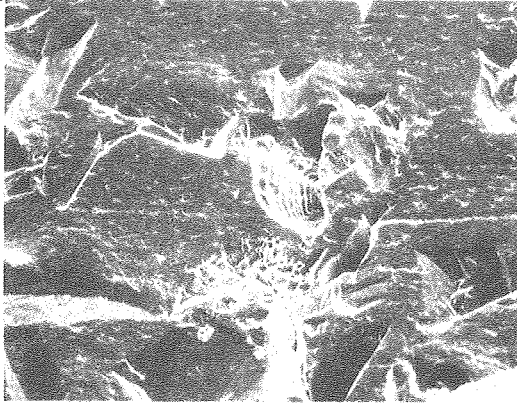
D

10 μ m

0.4 g

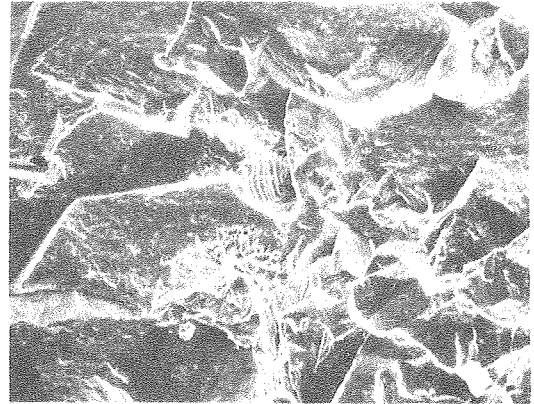
Fig.6

XBB 790-13300A



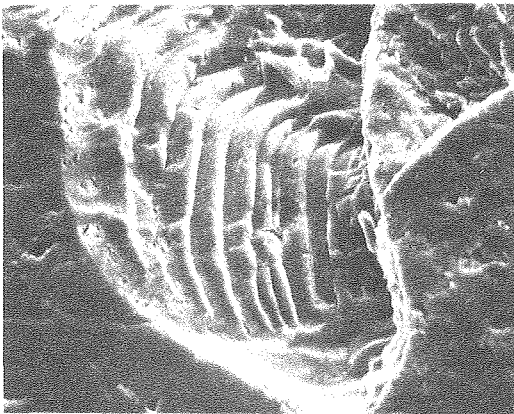
0.3 g

50 μ m



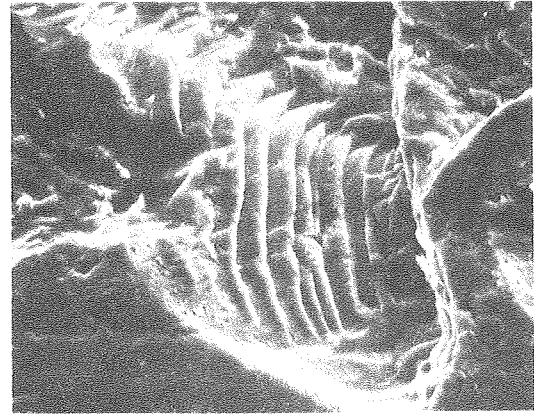
0.4 g

50 μ m



0.3 g

10 μ m

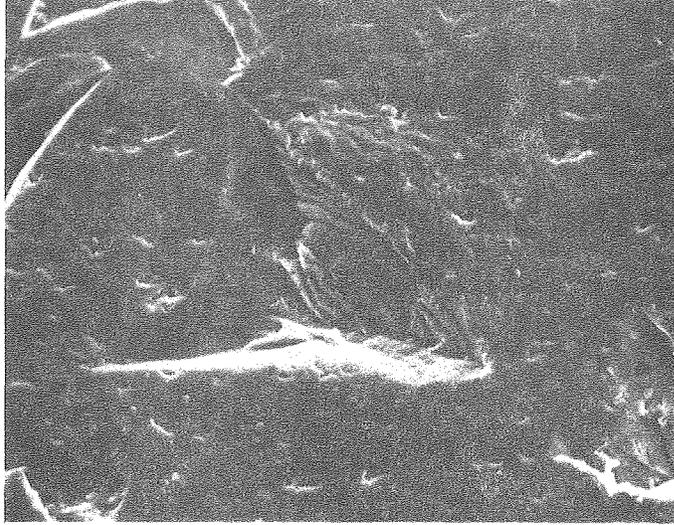


0.4 g

10 μ m

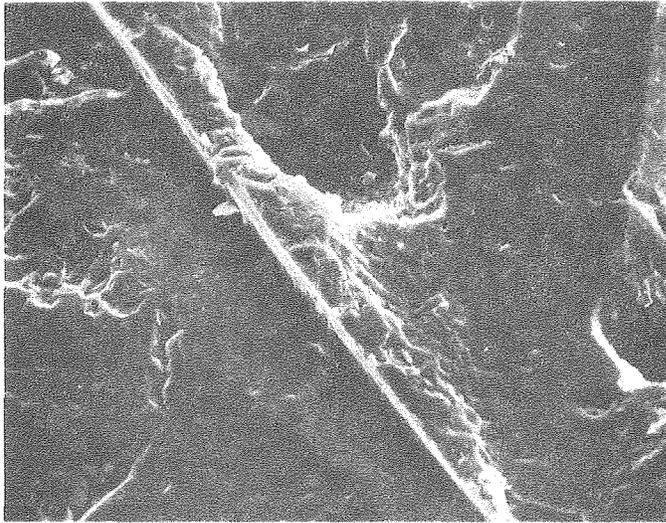
Fig. 7

XBB 790-13301A



50 μm

Fig. 8



10 μm

Fig. 9

XBB 806-17865

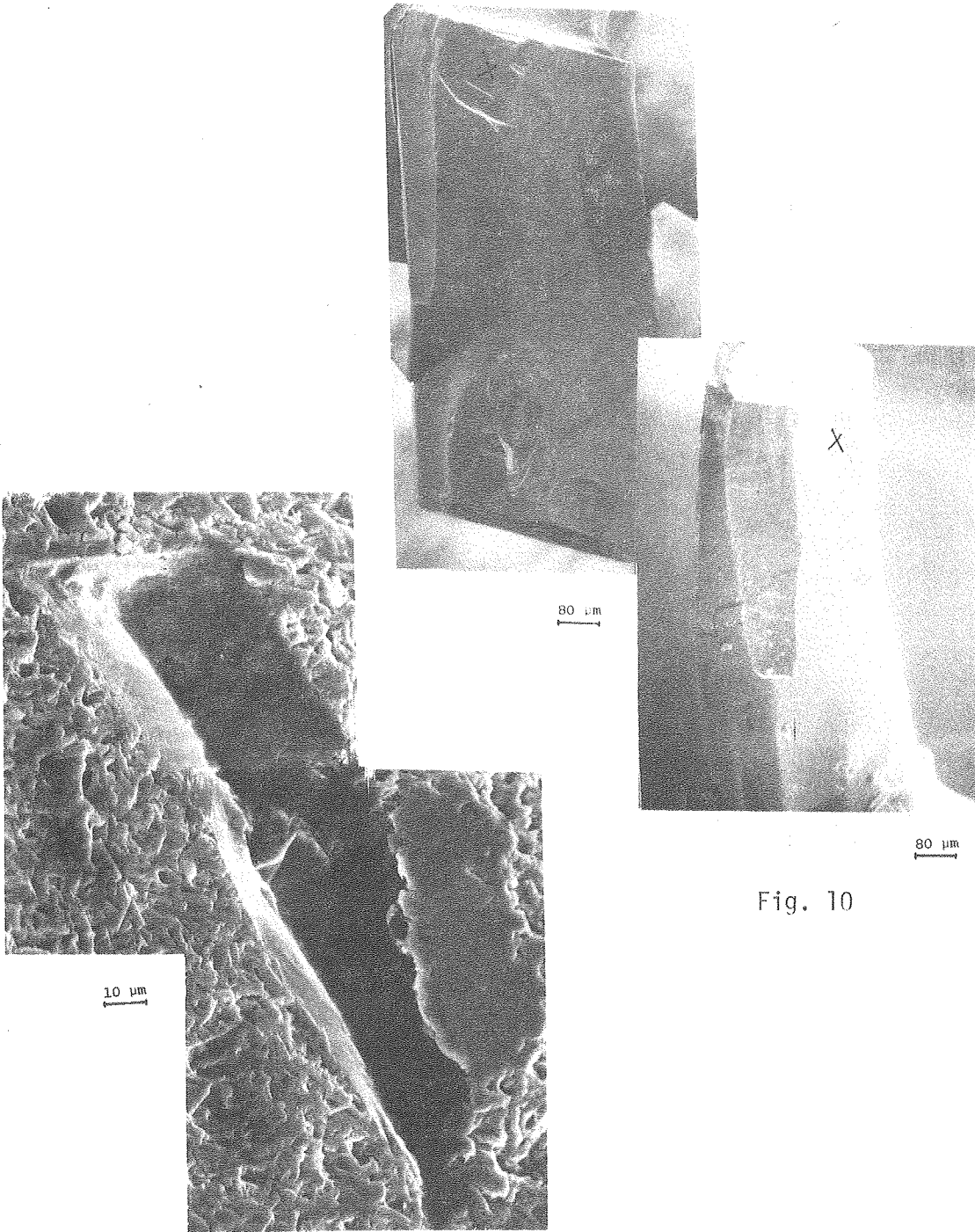


Fig. 10

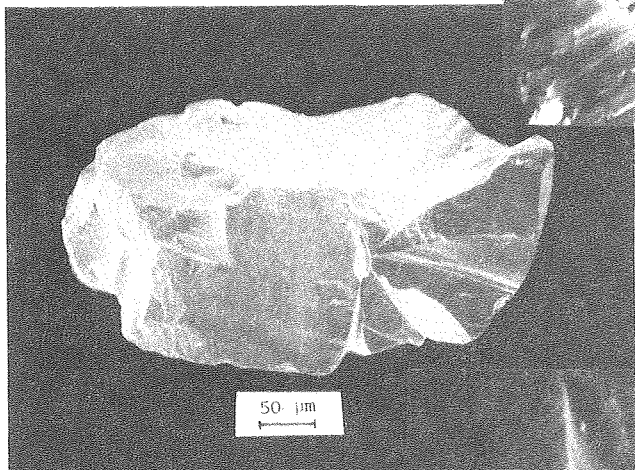
Fig. 11

XBB 806-7869



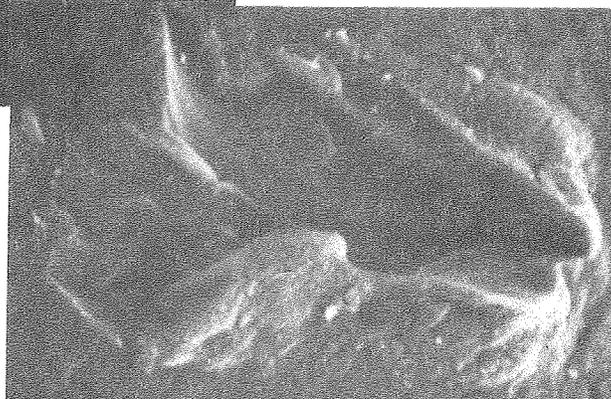
Fig. 12

1 μm



50 μm

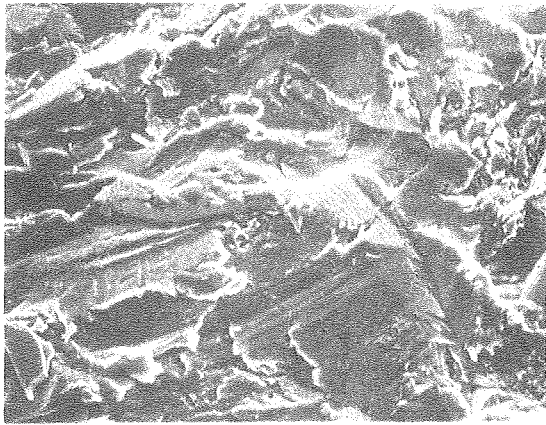
Fig. 13



5 μm

Fig. 14

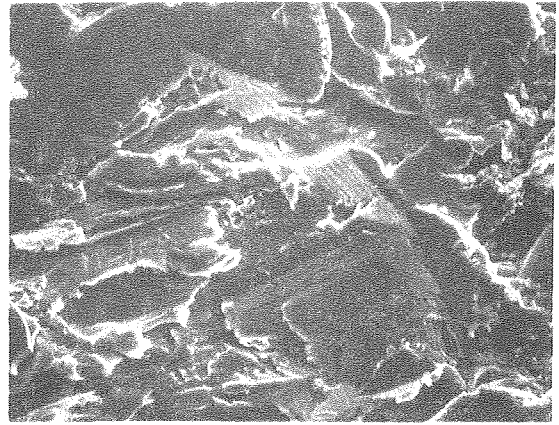
XBB 806-7867



A

20 μm

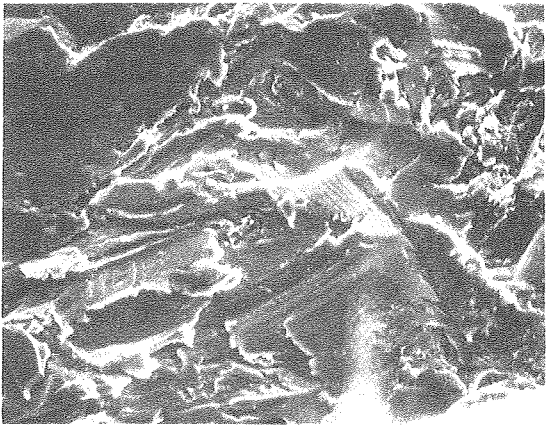
0.4 g



C

20 μm

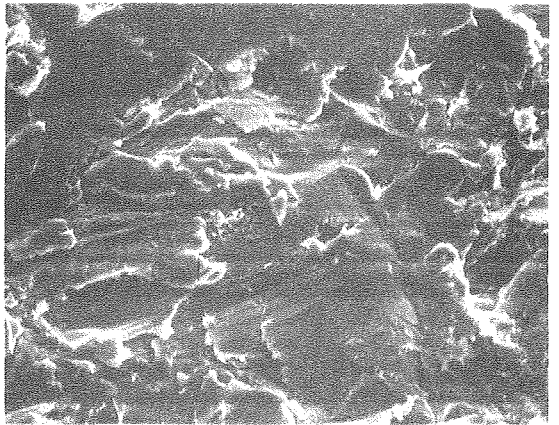
1.2 g



B

20 μm

0.8 g



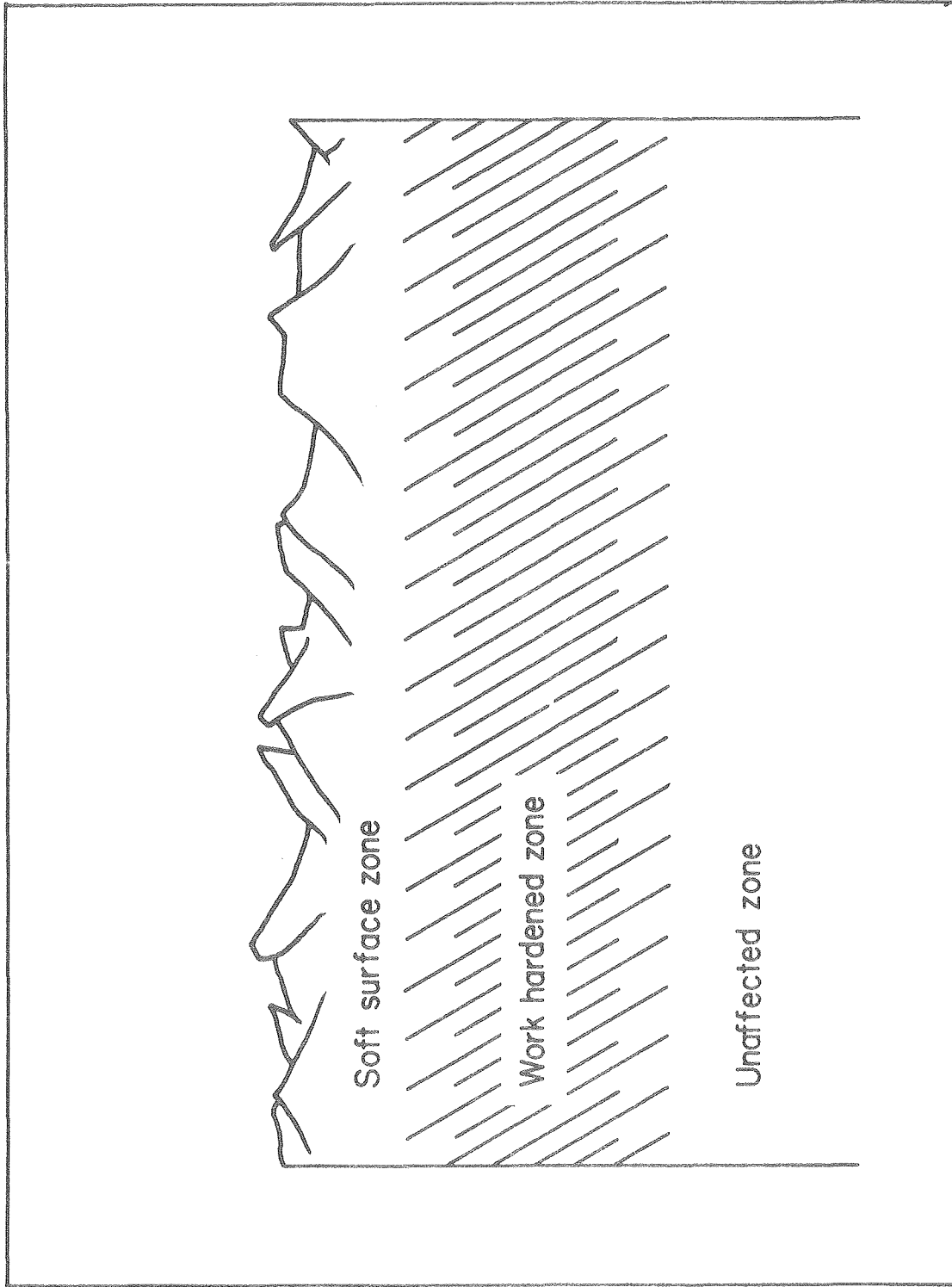
D

20 μm

1.6 g

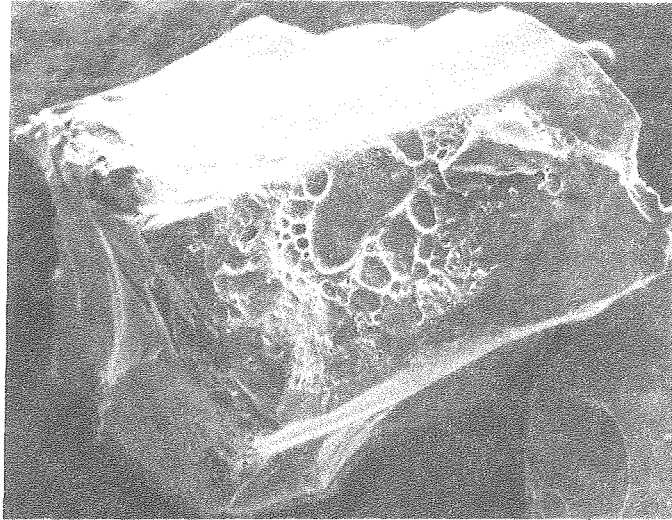
Fig. 15

XBB 790-13299A

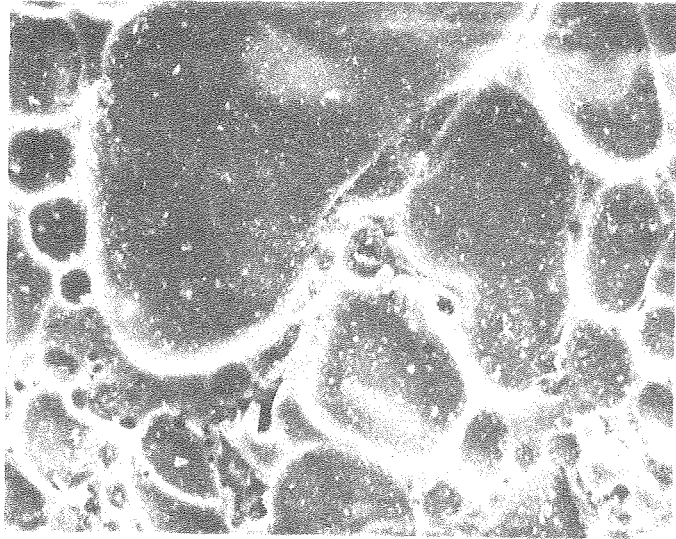


XBL 807-10669

Fig. 16



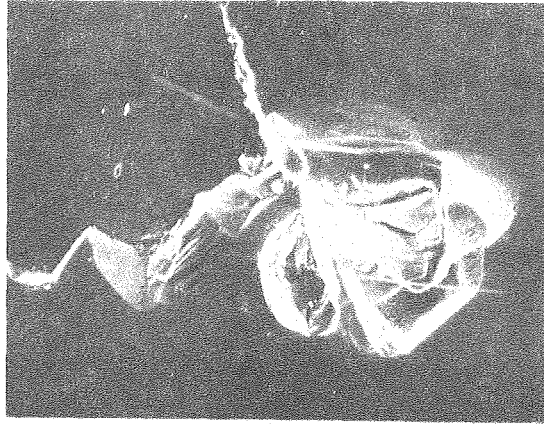
200 μ m



40 μ m

Fig. 17

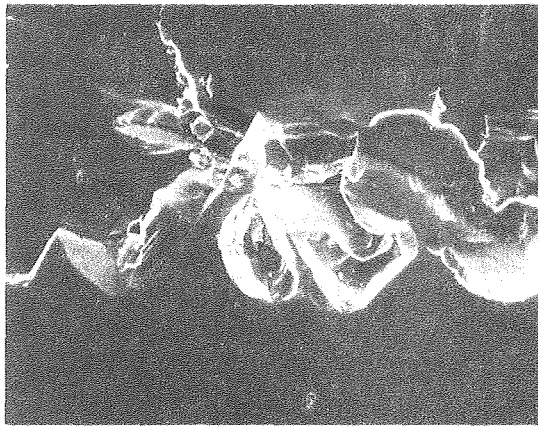
XBB 806-7863



A

20 μ m

0.1 g



B

20 μ m

0.2 g



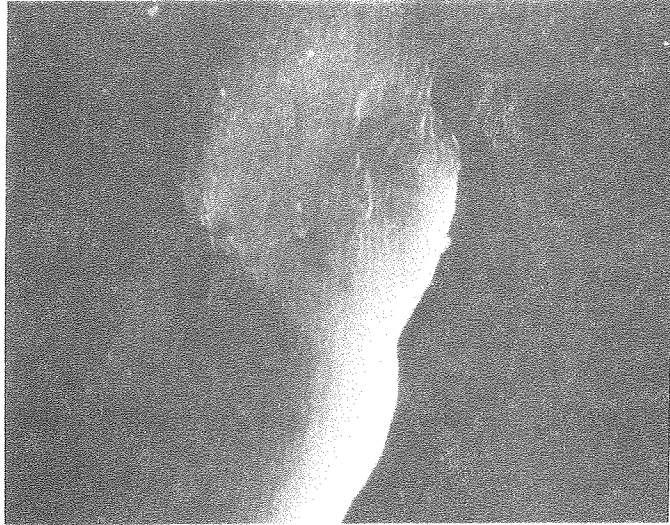
C

20 μ m

0.3 g

Fig. 18

XBB 790-13302A



1 μ m

Fig. 19

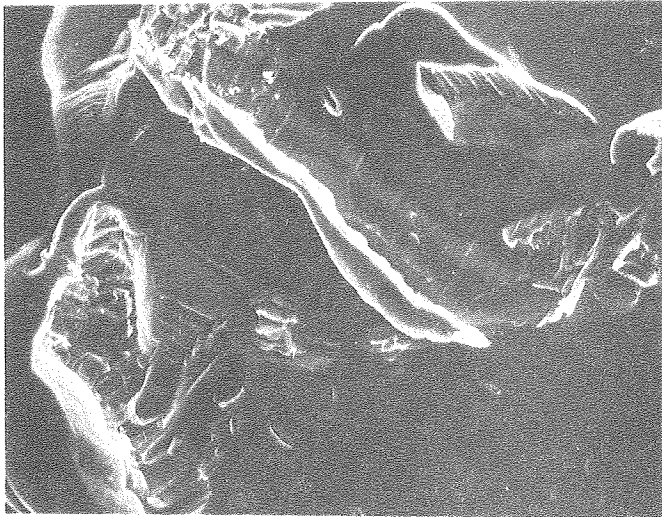
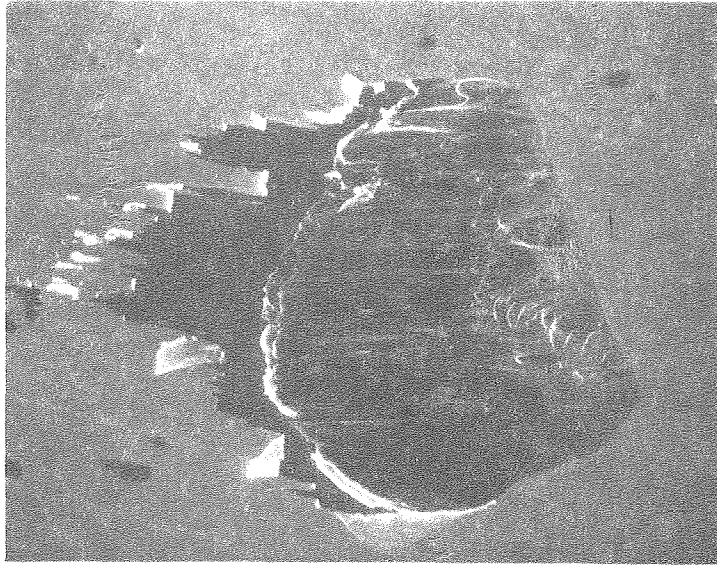


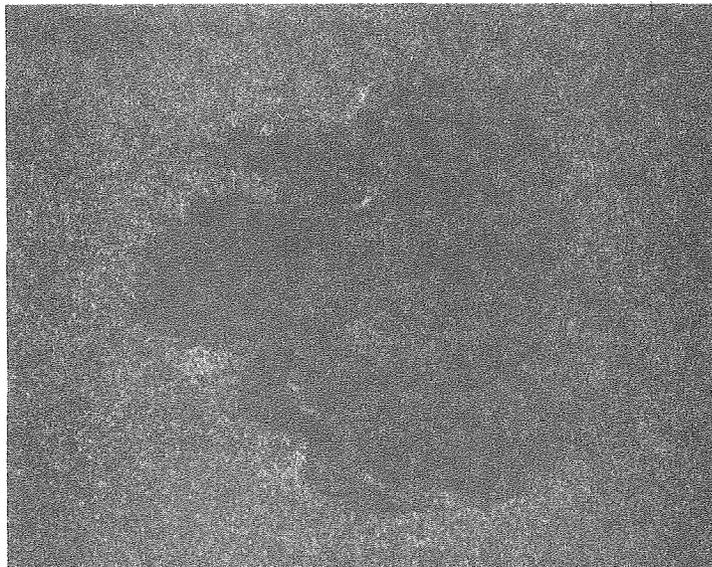
Fig. 20

XBB 806-7862



20 μ m

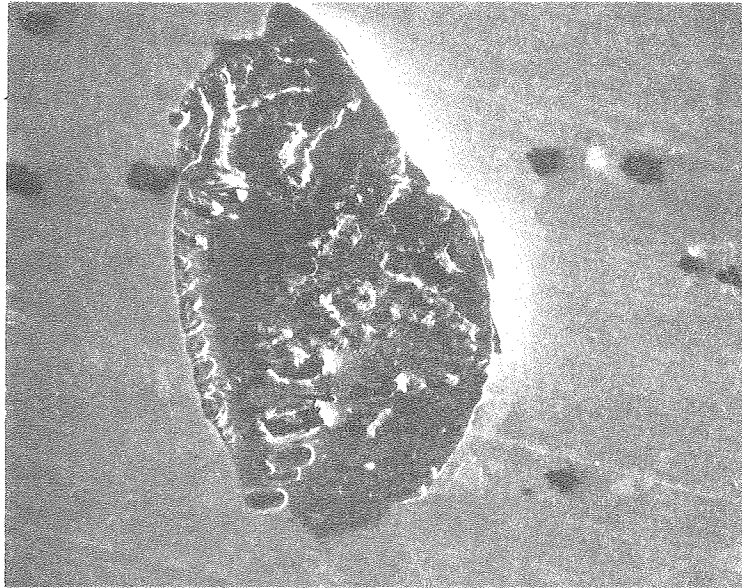
← IMPACT DIRECTION →



GOLD MAP

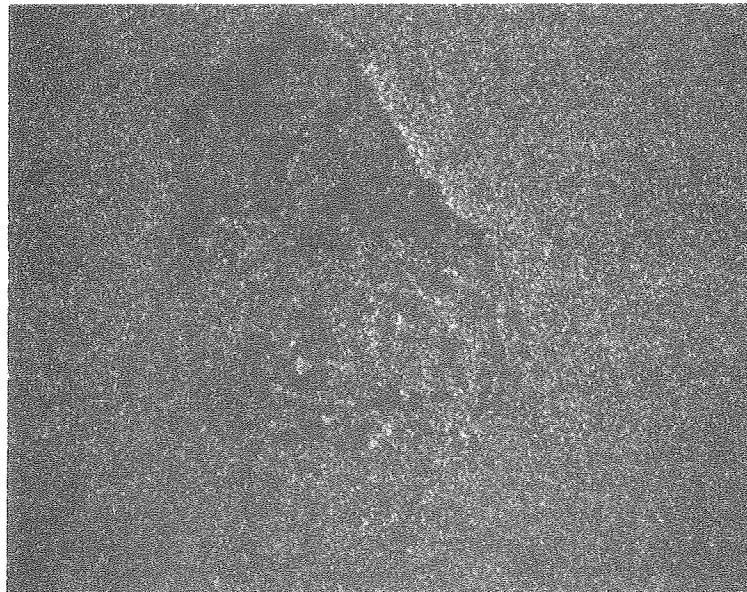
Fig. 21

XBB 806-7861



20 μm

————— IMPACT DIRECTION —————>



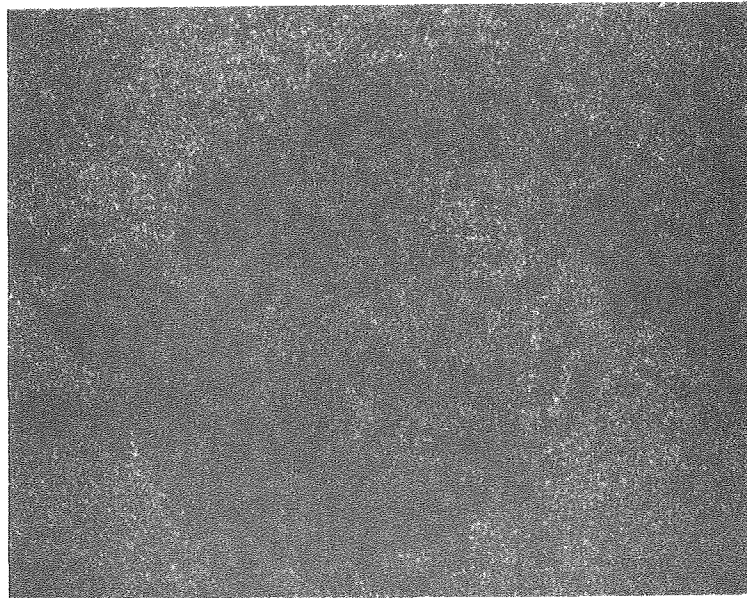
GOLD MAP

Fig. 22

XBB 790-13304A



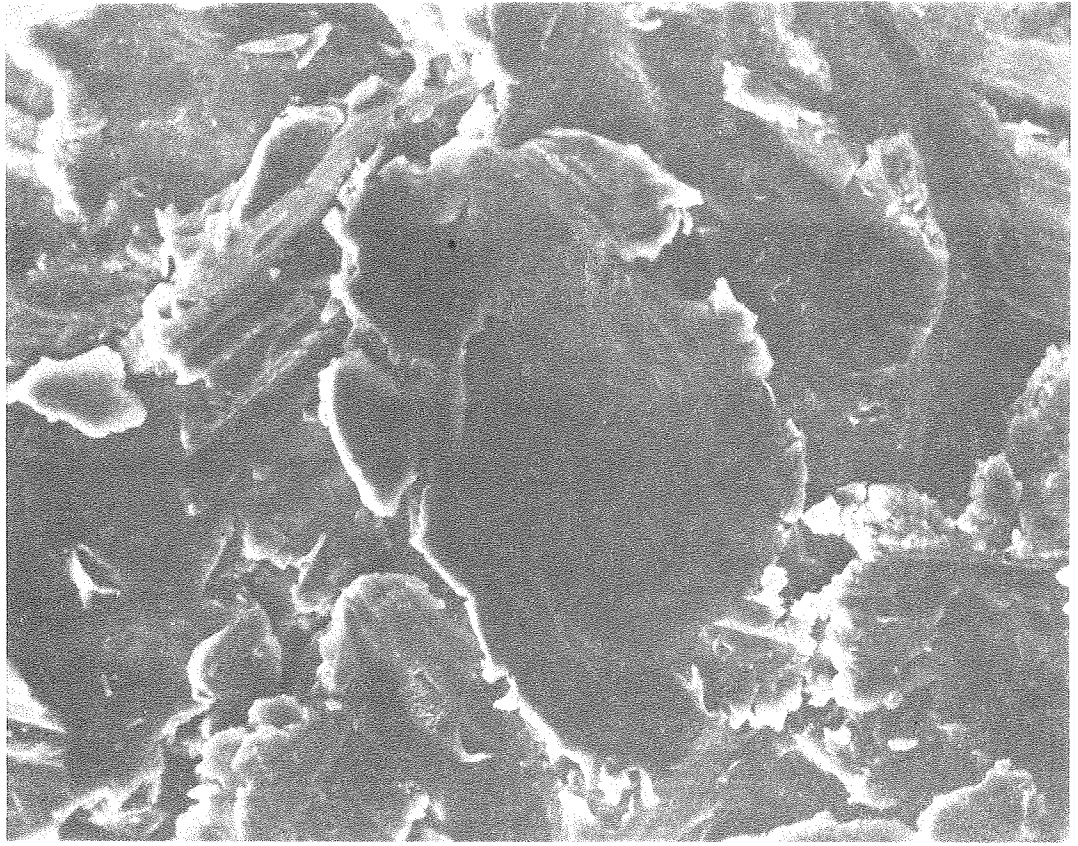
10 μm



GOLD MAP

Fig. 23

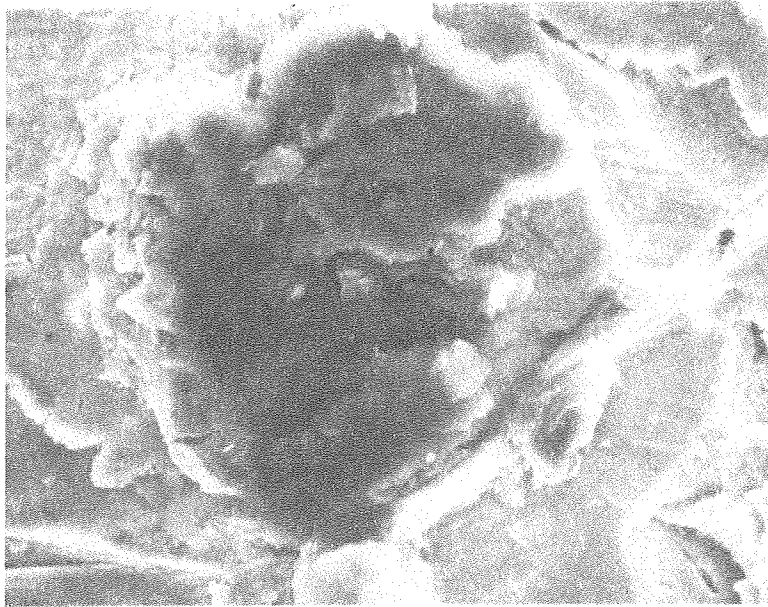
XBB 790-13303A



10 μm
└──────────┘

Fig. 24

XBB 806-7866

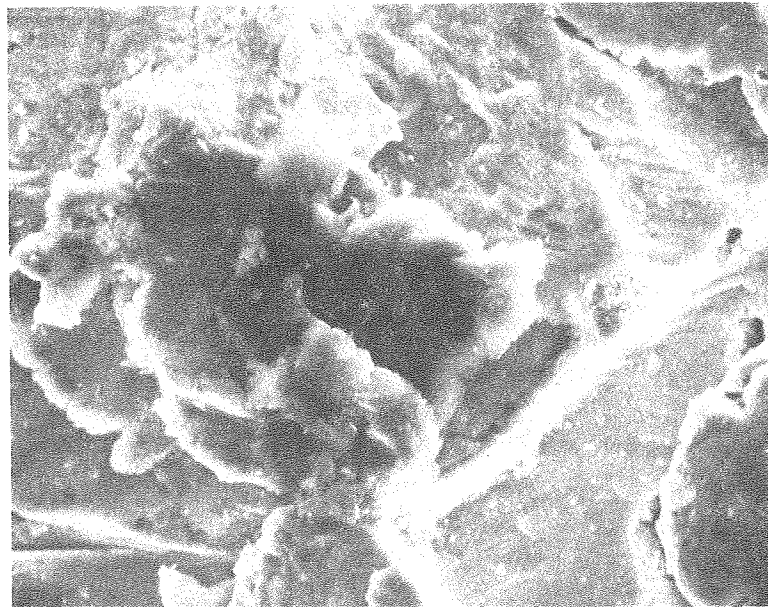


A

10 μm

1g

← IMPACT DIRECTION →



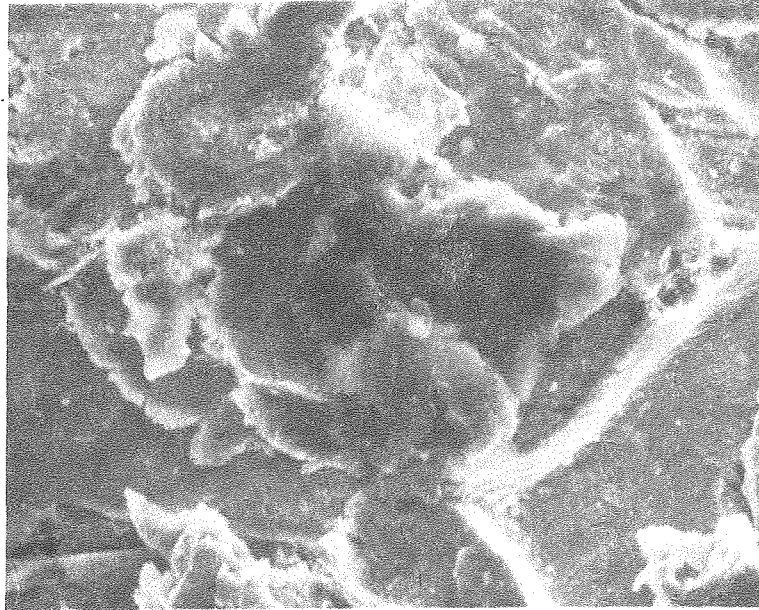
B

10 μm

2g

Fig. 25

XBB 790-13307A

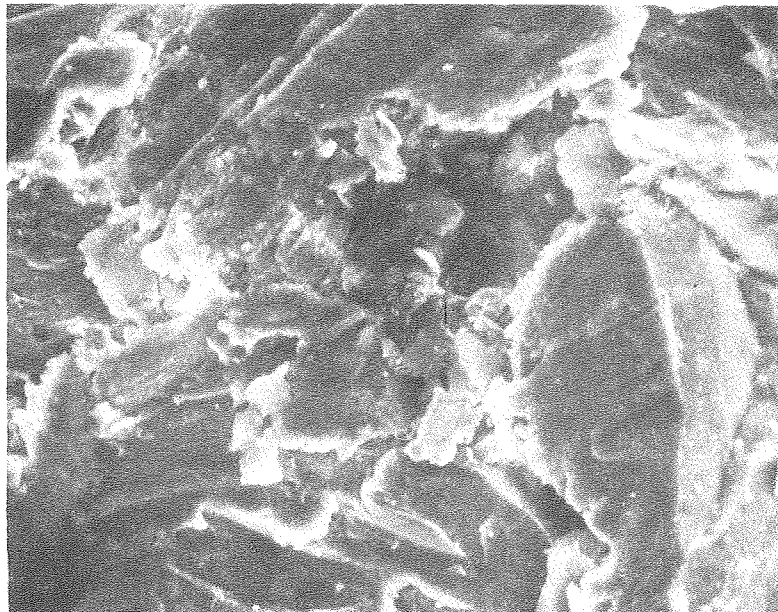


A

10 μm

3g

← IMPACT DIRECTION →



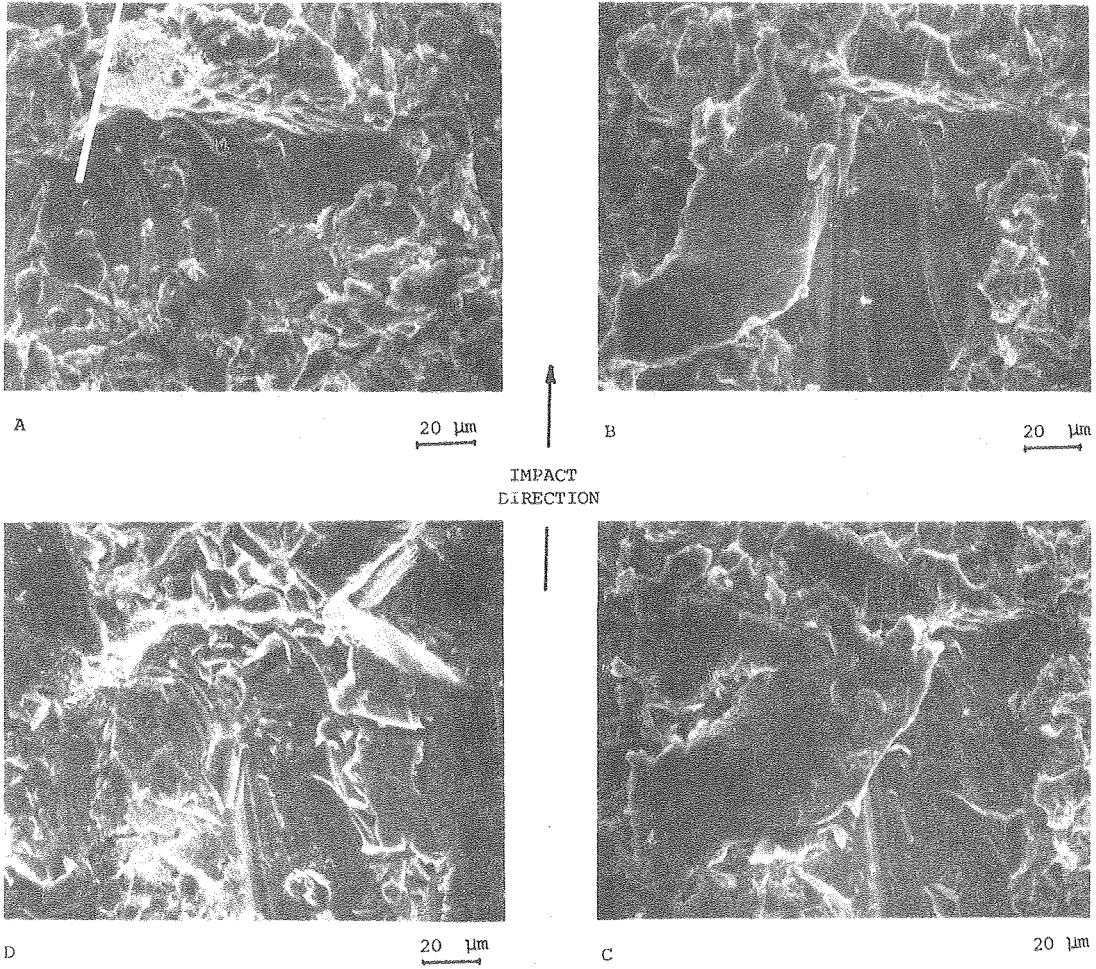
B

10 μm

4g

XBB 806-7864

Fig. 26



XBB 801-1299A

Fig. 27